EFFECT OF FLUE GAS IMPURITIES ON THE PROCESS OF INJECTION AND STORAGE OF CARBON DIOXIDE IN DEPLETED GAS RESERVOIRS

A Thesis

by

MARJORIE C. NOGUEIRA DE MAGO

Submitted to the Office of Graduate Studies of
Texas A&M University
in partial fulfillment of the requirements for the degree of

MASTER OF SCIENCE

August 2005

Major Subject: Petroleum Engineering

EFFECT OF FLUE GAS IMPURITIES ON THE PROCESS OF INJECTION AND STORAGE OF CARBON DIOXIDE IN DEPLETED GAS RESERVOIRS

A Thesis

by

MARJORIE C. NOGUEIRA DE MAGO

Submitted to the Office of Graduate Studies of
Texas A&M University
in partial fulfillment of the requirements for the degree of

MASTER OF SCIENCE

Approved by:

Chair of Committee,	Daulat D. Mamora
Committee Members,	Maria A. Barrufet
	Ben Welch
Head of Department,	Steve Holditch

August 2005

Major Subject: Petroleum Engineering

ABSTRACT

Effect of Flue Gas Impurities on the Process of Injection and Storage of Carbon Dioxide in Depleted Gas Reservoirs. (August 2005)

Marjorie C. Nogueira de Mago, B.S., Simon Bolivar University

Chair of Advisory Committee: Dr. Daulat D. Mamora

Previous experiments - injecting pure CO_2 into carbonate cores - showed that the process is a win-win technology, sequestrating CO_2 while recovering a significant amount of hitherto unrecoverable natural gas that could help defray the cost of CO_2 sequestration. In this thesis, I report my findings on the effect of flue gas "impurities" on the displacement of natural gas during CO_2 sequestration, and results on unconfined compressive strength (UCS) tests to carbonate samples.

In displacement experiments, corefloods were conducted at 1,500 psig and 70°C, in which flue gas was injected into an Austin chalk core containing initially methane. Two types of flue gases were injected: dehydrated flue gas with 13.574 mole% CO_2 (Gas A), and treated flue gas (N_2, O_2 and water removed) with 99.433 mole% CO_2 (Gas B). The main results of this study are as follows. First, the dispersion coefficient increases with concentration of "impurities". Gas A exhibits the largest dispersion coefficients, 0.18-0.25 cm^2/min, compared to 0.13-0.15 cm^2/min for Gas B, and 0.15 cm^2/min for pure CO_2. Second, recovery of methane at breakthrough is relatively high, ranging from 86% OGIP for pure CO_2, 74-90% OGIP for Gas B, and 79-81% for Gas A. Lastly, injection of Gas A would sequester the least amount of CO_2 as it contains about 80 mole% nitrogen. From the view point of sequestration, Gas A would be least desirable while Gas B appears to be the most desirable as separation cost would probably be cheaper than that for pure CO_2 with similar gas recovery.

For UCS tests, corefloods were conducted at 1,700 psig and 65°C in such a way that the cell throughput of CO_2 simulates near-wellbore throughput. This was achieved through increasing the injection rate and time of injection. Corefloods were followed by porosity measurement and UCS tests. Main results are presented as follows. First, the UCS of the rock was reduced by approximately 30% of its original value as a result of the dissolution process. Second, porosity profiles of rock samples increased up to 2.5% after corefloods. UCS test results indicate that CO_2 injection will cause weakening of near-wellbore formation rock.

I dedicate this thesis to:

My husband: *Alonso Luis Mago*

and

My parents: *Julio Nogueira*
Marjorie Gimenez

Thanks for giving me your support,
love, and guidance through
this entire journey.

ACKNOWLEDGEMENTS

I would like to give special thanks to my advisor and chair of my M.S. committee, Dr. Daulat D. Mamora for his continuous guidance, advice, support, enthusiasm, and encouragement throughout my research and education at Texas A&M University.

I also wish to thank Dr. Maria Barrufet and Dr. Ben Welch for their support and useful discussions during the course of this research and for serving as members of my graduate advisory committee.

I would like to thank my husband, Alonso, for being there for me through all my research. Thanks for supporting me through the long hours in the laboratory to successfully accomplish my experiments.

Thanks to my family living in Venezuela, Julio, Marjorie, Irma, Alonso Dimas, Daisy, and Ricardo for loving me and for giving me the courage to work hard every day. Thanks to my grand mother “abuela Daisy” for making a special effort to come to College Station to visit us from Venezuela.

It has been a pleasure to work with all members of Dr. Mamora’s research group, especially with Jose Antonio. I want to express my gratitude to Jose Antonio and Meiling Rivero for always helping me.

I would like to thank the professors and staff at the Petroleum Engineering Department at Texas A&M University for all of their support. I would also like to thank the faculty and staff at the Civil Engineering Department for opening their facilities to me and for giving me quality time to run unconfined compressive strength tests in their Structural and Materials laboratory. Last, I wish to express my gratitude to the U.S. Department of Energy for sponsoring this study.

TABLE OF CONTENTS

Page

CHAPTER Page

LIST OF FIGURES

LIST OF TABLES

CHAPTER I

INTRODUCTION

1.1 Present Status of the Question

Depleted gas reservoirs provide favorable conditions for the sequestration of large volumes of carbon dioxide. In addition, repressurization and displacement of natural gas by CO_2 results in the recovery of significant amounts of unrecoverable gas reserves defraying the cost of carbon dioxide sequestration. Previous experiments with CO_2 have shown that displacement of natural gas by supercritical CO_2 is a very efficient process.[1] However, CO_2 sources are rarely pure. The cost of CO_2 separation out of flue gas is significantly higher than that of transporting and injecting it into reservoirs. In practice, flue gas impurities such as SO_2, NO_2, CO, O_2 and N_2 are present in the CO_2 stream to be sequestered.[2] Therefore, effects of these impurities on CO_2 displacement efficiency need to be investigated.

To make geologic sequestration of greenhouse gases an environmentally acceptable practice, it is necessary to understand how geologic formations will react to pre- and post-operational conditions, with a focus on the formations around the wellbore. The structural integrity of a reservoir formation is important not only to ensure that the gas does not return to the atmosphere gradually, but also because a sudden release of carbon dioxide in a populated area could be catastrophic. If carbon dioxide is injected into a carbonate reservoir or carbonate-bearing sandstone reservoir, calcite dissolution could occur. Weakening of near-wellbore formation rock may result in subsidence and possibly wellbore collapse.[3]

This thesis presents the results of coreflood experiments in which a CO_2 stream with impurities displaced C_1 at pressures and temperatures encountered in the field. An analytical model based on experimental results was developed in order to estimate the gain in gas recovery and sweep efficiency. Changes in the rock compressive strength of Austin limestone samples were measured after injecting CO_2 for a prolonged period of time into these reservoir rocks.

This thesis follows the style and format of the *Journal of Petroleum Technology.*

1.2 Objectives

The main objectives of this research are as follows:

- Evaluate experimentally the effect of flue gas impurities on CO_2 displacement efficiency of natural gas (methane) in Austin chalk core samples: C_1 recovery (% OGIP), breakthrough time, and dispersion coefficient of the injected CO_2 mixture.
- Quantify experimentally the effect of carbon dioxide injection on calcite dissolution and thus the change in compressive strength of the Austin chalk samples**.**

CHAPTER II

LITERATURE REVIEW

Carbon dioxide is one of the major contributors to the greenhouse effect. When the solar energy passes through the atmosphere, it heats the earth surface. Greenhouse gases trap some of this heat to keep the atmosphere warm. Greenhouse gases include CO_2, methane, water vapor, NO_2, and aerosols. Without the natural greenhouse effect, the average temperature of the earth's surface would be on the order of -2°F, rather than the 57°F actually observed.

Emissions from burning fossil fuels are the major contributor to the increase in atmospheric CO_2 levels that can potentially lead to global climate change. Environmentalists predict that the global surface temperature can rise 1 to 4.5 °F in the next 50 years, and 2.2 to 10°F in the next century.[2] In this respect, strategies to reduce or limit gaseous carbon production from fossil fuel use need to be developed.

Worldwide environmental concerns regarding greenhouse gases have resulted in new regulations to be passed and higher emission standards to be enforced. Under the Kyoto protocol, developed countries are committed to reduce emissions of greenhouse gases by an average of 5.2% below the 1990 levels by 2008 to 2012.[4] Under the Rio Treaty, the United States and other 160 countries target to stabilize greenhouse gas concentrations in the atmosphere within a time frame sufficient to allow ecosystems to adapt, to ensure food production and to enable a sustainable economic development.[5] On November 2003, U.S. DOE proposed General Guidelines for the voluntary reporting of greenhouse gas emissions and emission reductions, scheduled for release in fall 2004. In the future, greenhouse gas emission reporting will be mandatory; hence, a more efficient use of energy and the development of new technologies will be required to meet the challenge of stabilizing CO_2 concentrations in the atmosphere.

2.1 Geologic Sequestration of CO_2

Possible CO_2 sequestration sites (**Fig. 2.1**) include coal beds, depleted gas an oil reservoirs, deep aquifers, salt domes and the deep ocean floors. Geologic sequestration of CO_2 appears to be a reasonable pathway to stabilization of atmospheric CO_2 concentration. The various options must be evaluated for cost, safety, and environmental effects. Our ongoing study is the evaluation of CO_2 storage in depleted gas reservoirs.

The principal motivation for injecting CO_2 in geologic formations has been to maximize CO_2 storage volume and to enhance hydrocarbon recovery. This is the case of CO_2 injection in oil reservoirs and unmineable coal beds. The first large-scale project specifically aimed at CO_2 underground disposal was started in 1996 by Statoil in the North Sea.[6,7] Approximately $1x10^6$ tonnes per year of CO_2 from the Sleipner Vest field are separated out of the produced natural gas and injected into the overlying Utsira aquifer. This project demonstrated the feasibility of sequestering CO_2 in saline aquifers. More recently, a combined EOR and CO_2-sequestration project has been undertaken, in which CO_2 generated at a coal-gasification plant in North Dakota is transported by pipeline to the Weyburn field in Saskatchewan to be injected.[8] This is the first attempt to sequester CO_2 in an oil reservoir.

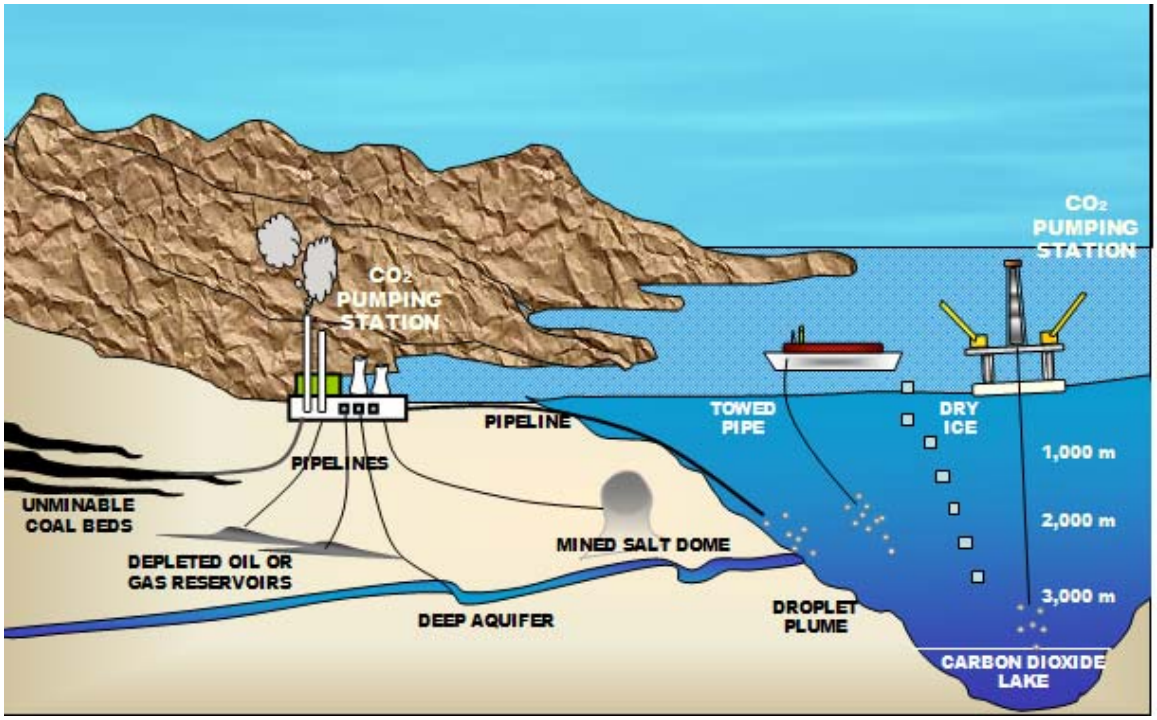

Fig. 2.1—Storage sites for CO_2 in geologic formations and the deep sea.

Carbon dioxide injection into gas reservoirs has been proposed but not tested. CO_2 could be used for pressure maintenance or for condensate vaporization, but the cost of purchasing CO_2 makes this approach uneconomical in the absence of incentives for CO_2 storage.[6]

Given a depleted natural gas reservoir and a depleted oil reservoir with the same hydrocarbon pore volume, the depleted natural gas reservoir will store significantly more CO_2. This is due to the high compressibility of natural gas (approximately 30 times more compressible than oil and water), and the fact that the ultimate hydrocarbon recovery in a gas reservoir is typically about twice as large as that in an oil reservoir.[9] In addition to the larger storage capacity of depleted gas reservoirs, another advantage is that all CO_2 - resulting from the combustion of natural gas produced from the reservoir - could be stored in the same reservoir, with additional storage capacity. For each mole of C_1 combusted, one mole of CO_2 is produced, and the molar volume of CO_2 is smaller than that of C_1 at the same field temperature and pressure. Therefore, CO_2 injection could be replaced for a mixture of CO_2, N_2 and impurities resulting from the partial separation of flue gas.[6]

2.2 CO_2 Capture

Unfortunately, CO_2 sources are rarely pure; the most likely CO_2 source is usually a stream extracted from the flue gas of a power plant.[10] Flue-gas composition from typical electric power generation plants depends on the fuel type (bituminous coal, natural gas, wet feed of slurry coal, etc), amount of excess air, and power generation scheme (boiler, steam, and gas turbine types).

A typical flue-gas composition of an electric power plant based on a combustion calculation for a Powder River Basin (PRB) coal in a 500 MW plant with 20% excess air, is shown in **Table 2.1**. The main components of flue gas are N_2 (71 mole %), CO_2 (12 mole %), H_2O (12 mole %), O_2 (5 mole %), and also impurities such as SO_2, NO_2, and CO.* Flue gas may be treated to obtain a stream rich in CO_2 for sequestration purposes. Two types of treated flue gases are used in my experiments: dehydrated flue gas with 13.574 mole % CO_2 (Gas A), and treated flue gas with 99.433 mole % CO_2 (Gas B) as presented in Table 2.1

According to the International Environmental Agency (IEA), the total cost of CO_2 capture and storage ranges from $50 to $100/tonne of CO_2.This cost can be split into cost of capture, transportation and storage. Current estimates for large-scale capture systems (including CO_2 pressurization, excluding transportation and storage) are $25 to $50/tonne of CO_2. Transportation

* Electronic communication with D. Chuck, EPRI-Continuous and Predictive Emissions Monitoring Group (22 July 2003).

costs are approximately \$1 to \$5/tonne of CO_2 per 100 km, and storage costs are \$1 to \$2/tonne of CO_2. [11,12] Unquestionably, the cost of capturing CO_2 out of flue gas is significantly higher than that of transporting and injecting CO_2 in reservoirs.[3] Due to the high cost of CO_2 capture, the purpose of this study is to understand and model the displacement of natural gas by flue gas and compare it with the displacement by pure CO_2. Results will determine if flue gas displacement efficiency will enhance gas recovery, and if flue gas sequestration in depleted gas reservoirs is an alternative for reducing CO_2 levels in the atmosphere.

TABLE 2.1—COMPOSITION OF FLUE GAS FROM AN ELECTRIC POWER GENERATION PLANT

		Composition, mole %	
Component	Flue Gas	Gas A	Gas B
Nitrogen, N_2	70.726	80.370	---
Water, H_2O	12.000	---	---
Carbon dioxide, CO_2	11.945	13.574	99.433
Oxygen, O_2	5.258	5.975	---
Sulfur dioxide, SO_2	0.045	0.051	0.368
Nitrogen oxide, NO_2	0.016	0.018	0.129
Carbon monoxide, CO	0.010	0.012	0.070
Total	100.000	100.000	100.000

2.3 Coreflood Experiments Injecting "Pure" CO_2 in Carbonate Rocks

Previous coreflood experiments injecting pure CO_2 into carbonate rocks showed that the process is a win-win technology, sequestrating CO_2 while recovering significant amounts of hitherto unrecoverable natural gas that could help defray the cost of CO_2 sequestration.

Seo and Mamora (2004) concluded that displacement of C_1 by CO_2 –whether CO_2 is a gas, liquid or supercritical fluid –appears to be a very efficient process. In addition, at experimental conditions (20 to 80 ^oC and 1,000 to 2,700 psi) the coefficient of longitudinal dispersion of CO_2 in

C_1 is relatively low, 0.01 to 0.30 cm^2/min; recovery of C_1 at CO_2 breakthrough is high, 73% to 87% of original gas in place (OGIP).[9,13,14] Experimental results at pressures and temperatures similar to the experiments presented in this thesis are presented in **Table 2.2**, and will be used as a reference to compare flue gas displacement efficiency with that of pure CO_2.

TABLE 2.2—EXPERIMENTAL DATA USING SUPERCRITICAL CO_2 IN COREFLOOD EXPERIMENTS AT 1,200 TO 1,700 PSI AND 60 TO 80 °C [9,13]

P, psig	T, °C	S_{wi}, fraction	OGIP, std L	C_1 recovery at breakthrough, %OGIP	Breakthrough, min	K_L, cm^2/min
1,200	60	0.0	3.604	86.80%	55.0	0.06
1,200	80	0.0	2.850	84.60%	30.0	0.30
1,700	60	0.0	5.202	86.80%	90.0	0.08
1,700	80	0.0	4.045	83.90%	60.0	0.17
1,700	80	0.2	3.739	61.80%	55.0	0.15

2.4 Analytical Model

The following convection-dispersion-reaction equation describes the overall transport and reaction of carbon dioxide for one-dimensional flow.[13]

$$K_L \frac{\partial^2 C}{\partial x^2} - v\frac{\partial C}{\partial x} - C_R = \frac{\partial C}{\partial t} \quad \text{.....(2.1)}$$

where C is the concentration of carbon dioxide at time t and location x, C_R is the reaction rate concentration of carbon dioxide with the reservoir, K_L is the coefficient of longitudinal dispersion, and v is the interstitial velocity of carbon dioxide. If the kinetic reaction term in **Eq. 2.1** is removed, we obtain the well-known convection-dispersion equation as given by **Eq. 2.2**.

$$K_L \frac{\partial^2 C}{\partial x^2} - v\frac{\partial C}{\partial x} = \frac{\partial C}{\partial t} \quad \text{.....(2.2)}$$

Eq. 2.2 may be expressed in dimensionless form as follows:

$$\frac{1}{P_e}\frac{\partial^2 C}{\partial x_D{}^2} - \frac{\partial C}{\partial x_D} = \frac{\partial C}{\partial t_D} \quad \text{..... (2.3)}$$

where:

$x_D = \frac{x}{L}$, dimensionless distance, where L is length of core,

$t_D = \frac{tv}{L}$, dimensionless time, and

$P_e = \frac{vL}{K_L}$, Peclet number (ratio of convection to dispersion).

Since the carbon dioxide injection inlet is at $x = 0$, then

Initial condition: $C = 1$ at $t_D = 0$,

Boundary conditions: $C = 1$ at $x_D = 0$, $t_D > 0$

$C \rightarrow 0$ as $x_D \rightarrow \infty$, $t_D > 0$

Solution to **Eq. 2.3** is presented below.

$$C = \frac{1}{2}\left\{\text{erfc}\left(\frac{x_D - t_D}{2\sqrt{t_D / P_e}}\right) + e^{P_e x_D}\,\text{erfc}\left(\frac{x_D + t_D}{2\sqrt{t_D / P_e}}\right)\right\} \quad \text{..... (2.4)}$$

Carbon dioxide concentration profiles are compared against those based on the analytical solution (**Eq. 2.4**) for various values of the dispersion coefficient. The correct dispersion coefficient would be that which gives the best agreement between data and the analytical solution.

2.5 Carbonate Dissolution

Carbon dioxide injection into carbonate formations could potentially cause weakening of near-wellbore formation rock. Carbon dioxide will react with the formation water resulting in the dissolution of carbonates and the formation of carbonic acid until equilibrium is reached between the fluids and the rock. The chemical equation that describes this reaction is as follows:

$$CO_2 + H_2O + CaCO_3 \Leftrightarrow Ca^{2+} + 2HCO_3^- \quad \text{..... (2.5)}$$

This equilibrium can be easily shift increasing the pH or in presence of high concentrations of aqueous metal cations, causing precipitation of secondary minerals, lowering permeability, porosity and potentially impeding further CO_2 injection. A pre-requisite for carbonate precipitation is the availability of non-carbonate minerals that will react with dissolved CO_2. This incorporation of CO_2 into a solid phase is referred as mineral trapping.[15]

Dr. John Morse in the Department of Oceanography at Texas A&M University found limited dissolution of carbonate occurred in cases where a small amount of connate water was present and found no more dissolution after equilibrium was reached between the fluid and rock.[16,17,18] However, if carbon dioxide is captured from the emissions of a power plant, the injection gas is likely to contain water and other impurities. Therefore, carbonate dissolution will occur through all the sequestration process potentially affecting the injectivity of the well and the integrity of the wellbore. Grigg reported that injectivity of CO_2 was the first concern of operators in the context of oil recovery by WAG process dealing with CO_2 particularly in open-hole wells.[19]

Izgec *et al*. concluded that changes in injectivity associated with rock permeability and porosity result from dissolution of rock minerals, transportation and later precipitation of them. Permeability and porosity alteration had similar trends in coreflood experiments with CO_2 and water in carbonate cores. They observed that as carbonic acid dissolves calcite and calcite particles deposit, the tortuosity should change continuously.[20]

Experimental results by Egermann *et al*. after coreflood experiments with CO_2-brine flow in carbonate rocks have shown that dissolution patterns, comparable to the wormholes during acidizing processes, have been observed. High flow rates give longer dissolution forms described as pinholes well distributed on the injection face, while low flow rates lead to a more compact dissolution described as limited number of big holes.[21]

Tristan *et al*. performed CO_2-brine flow experiments with carbonate cores and numerical simulation including reactive transport of CO_2. Their results indicated that dissolution of the rock is more severe at near the injection point and decreased as the fluid traveled into the formation.[22]

A most recent geochemical study performed by Knauss *et al*. considers the presence of flue gas impurities and other common industrial waste gases such as H_2S on the overall injection process. They found that the presence of H_2S negligibly affects the CO_2 injection process, but the presence of SO_2 can alter significantly the quantity of carbonates dissolved due to the formation of extremely low pH fluids.[23]

The geochemical modeling of carbonate dissolution and re-precipitation by CO_2 sequestration is a very complex process that highly depends on the rock compositions, reservoir fluids and the injected gas. This thesis doesn't cover the geochemistry behind the CO_2 injection process, but creates a scenario similar to that encountered near the wellbore in the field and evaluate changes on the integrity of the rock after CO_2 injection.

2.6 Compressive Strength Tests

To characterize the changes that occur in the strength of the rock after dissolution, the unconfined compression test is used widely.[24] Compressive strength σ_u is expressed as the ratio of peak load P_l to initial cross-sectional area A:

$$\sigma_u = \frac{P_l}{A} \quad \text{..... (2.6)}$$

Results from this type of test can vary by a factor of more than two as procedures are varied. The test sample should be a rock cylinder of length to width ratio in the range 2 to 2.5 with flat, smooth, parallel ends cut perpendicularly to the cylinder axis. Capping of ends with sulfur or plaster to achieve smoothness is suggested to introduce artificial end restraints that overly strengthen of the rock. However, introducing Teflon pads to reduce friction between the ends and the loading surfaces can cause premature splitting failure; especially in harder rocks.[24]

Procedures for this test are recommended in ASTM designation D2938. A typical report shall include the following information:

- Source of sample and lithologic description of the rock.
- Moisture condition before the test.
- Specimen diameter and height.
- Temperature at which test was performed.
- Rate of loading or deformation rate.
- Unconfined compressive strength.

- Type of failure; a sketch of the fractured specimen is recommended. **Fig 2.2** shows the different types of failure a specimen will present. Columnar fractures are typically encountered when the axial load is equally transmitted to the end of the specimen.

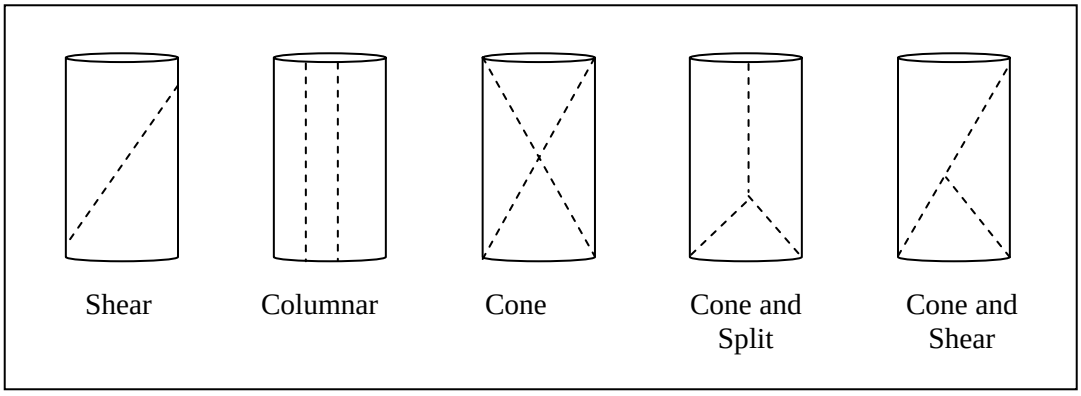

Fig. 2.2—Sketches of types of fracture.

Typical values for the compressive strength of a fresh sample of the Austin chalk formation may vary between 361 to 3,794 psi, with a mean value of 2,445 psi and a standard deviation of 727 psi. The carbonate content ranges between 62% and 92%. The specific gravity is approximately 2.68 ± 0.01.[25]

CHAPTER III

EXPERIMENTAL APPARATUS AND PROCEDURES

Two types of experiments were conducted in this research. First, displacement experiments were performed to determine the effect of impurities in the displacement efficiency of methane by CO_2. Second, compressive strength tests were performed to measure changes in the integrity of the rock after possible dissolution as a result of CO_2 injection. The experimental procedures will be described for each of the two types of experiments as well as equipment used.

3.1 Displacement Experiments

The main objective of these experiments is to measure the rate of longitudinal diffusion of CO_2 with impurities in gas-bearing carbonate reservoir rocks and compare the results with those obtained for pure CO_2. Parameters such as breakthrough time, recovery of original gas in place (OGIP), and compositions of the produced gas were measured to estimate the coefficient of longitudinal dispersion.

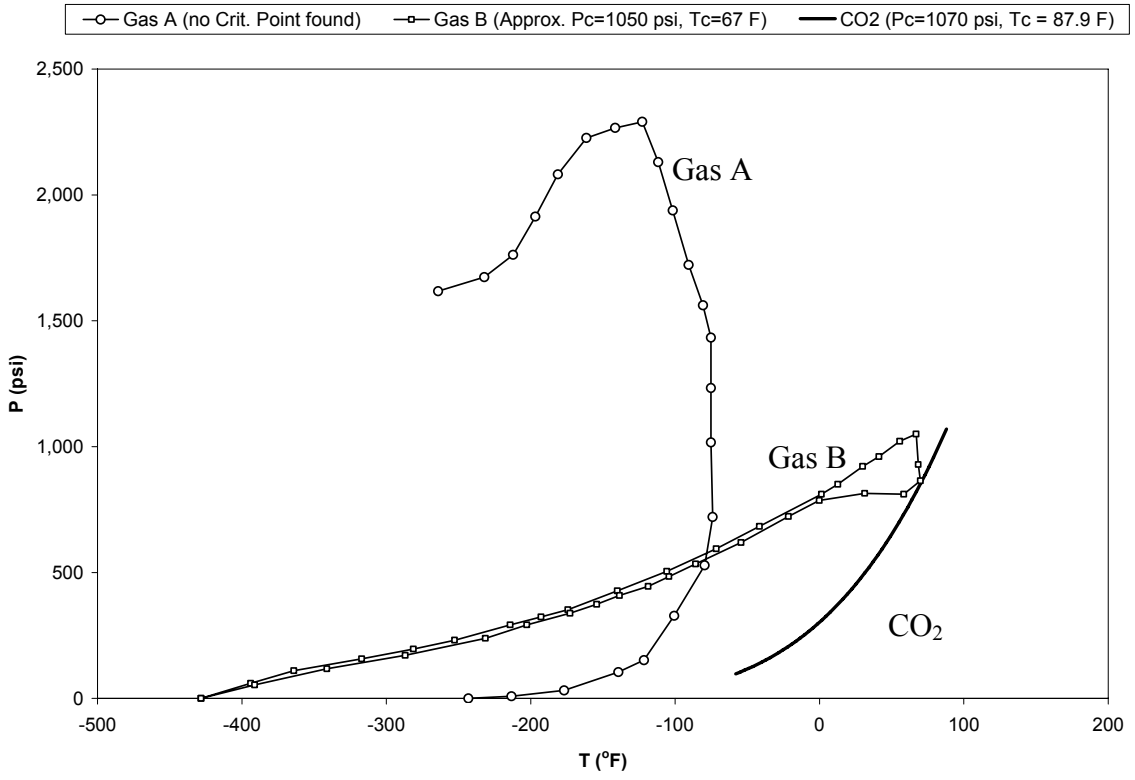

Fig. 3.1—Phase envelopes of injected gases compared to the CO_2 vapor pressure.

Two types of flue gases were used in these experiments: dehydrated flue gas with 13.574 mole % CO_2 (Gas A), and treated flue gas with 99.433 mole % CO_2 (Gas B) as presented in Table 2.1. The phase envelopes of the two gases (**Fig. 3.1**) were obtained from the company *Specialty Gas Products* of Houston that provided these reconstituted gases to our laboratory. No critical point was observed for Gas A.

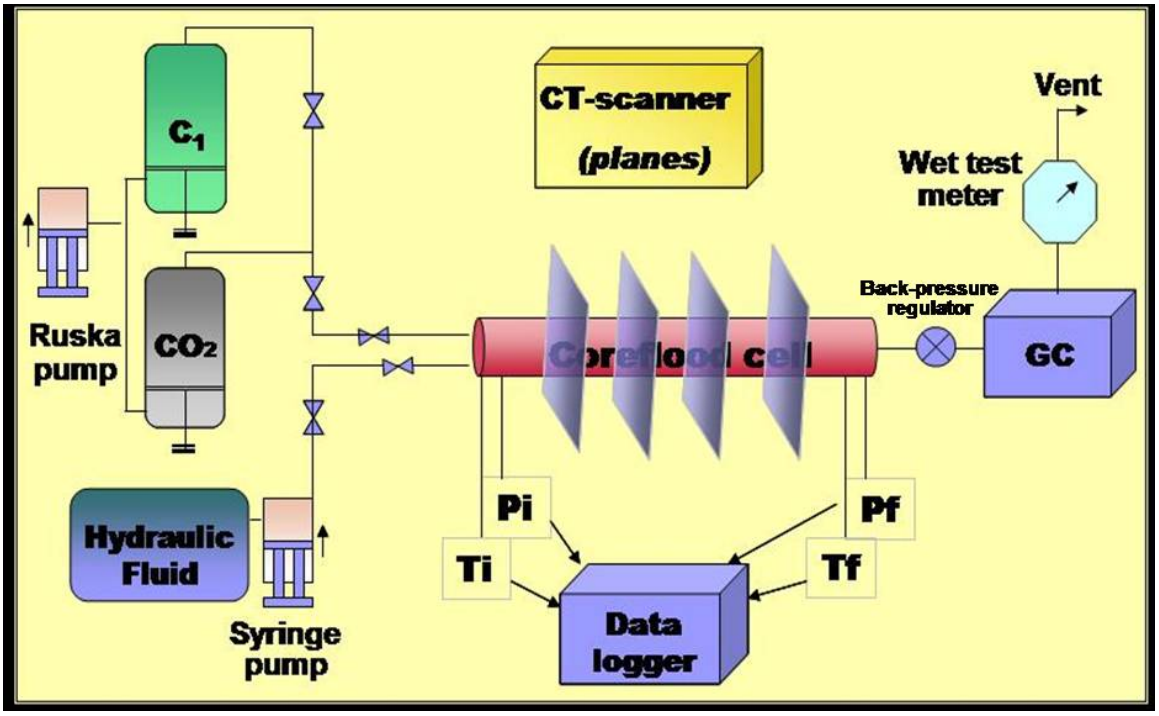

Fig. 3.2—Schematic diagram of experimental apparatus for displacement experiments.

The equipment used in these experiments consists of five main components: the injection system, the coreflood cell, the Universal System HD 350 x-ray computed tomography scanner (CT scanner), the production system and the data recording system. **Fig. 3.2** shows a diagram of the experimental apparatus, which is briefly described in the following. All of the equipment was available in the department of petroleum engineering at Texas A&M University.

3.1.1 Injection System

This consists of two sets of one-liter *Temco* accumulators connected to a *Ruska* pump (**Fig 3.3**) to displace the CO_2 gas mixture and the methane into the cell. After introducing each gas into the accumulator, the gas pressure is slowly increased to the desired level by injecting water below the piston in the accumulator.

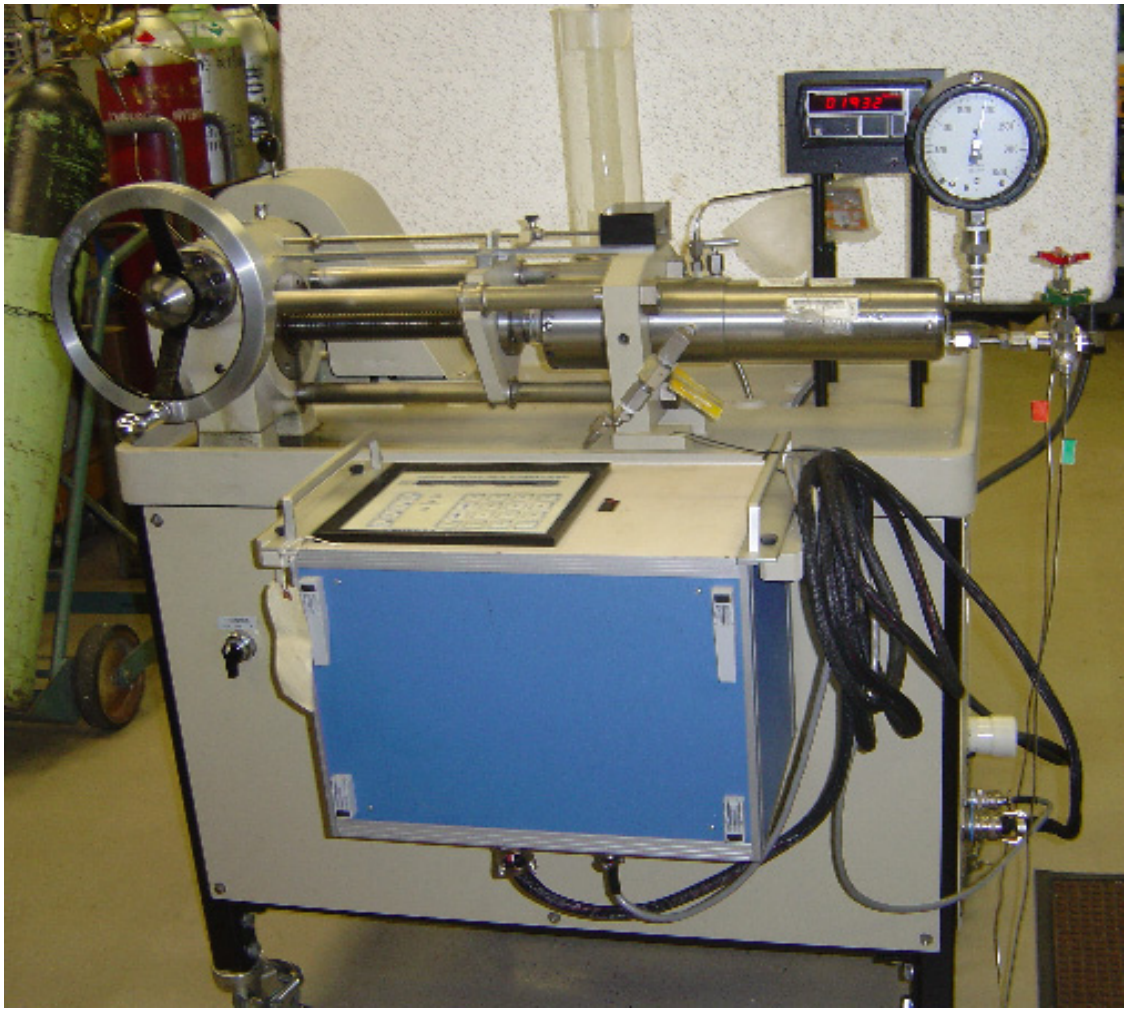

Fig. 3.3—*Ruska* pump used to pressurize and inject gases into the coreflood cell.

Table 3.1 lists the equipment used in the displacement experiments and compressive strength tests. A brief description of each of these main components follows.

TABLE 3.1—EQUIPMENT USED IN EXPERIMENTS

Equipment	Description
HPLC Pump	ISCO syringe pump, model 314, capacity 33.3cc/min
Accumulator	Temco, model CF50-200-66, max pressure 5,000 psi at 350°F
Pump	Ruska model 2216-603A, max pressure 10,000 psi, capacity 30 cc/min
Back Pressure Regulator	Tecom Corp., model 26-172224, max pressure 6,000 psi
Pressure Transducer	Omega, model PX 621, max pressure 10,000 psi
Thermocouple	Omega J-type
Coreflood Cell	Custom made, aluminum 7075-T6, 21 in long by 3.75 in OD with wall thickness of 1.91 in.
Convection Incubator	Precision, model 32 MR, temperature range 41 to 158°F
X-ray CT Scanner	Universal Systems, model HD-350 E
Wet Test Meter	American Meter Company, model P-2991
Data Logger	Hewlett-Packard data acquisition/switch unit, model 34970A
Gas Chromatograph	Hewlett-Packard series II model 5890
Integrator	Hewlett-Packard 3396A computing integrator
Manual Switching Valve	VICI switching valve for GC, model E36
Valve Actuator	VICI 2-position valve actuator, model DVSP4
Uniaxial Compression	MTS model 309.30S, maximum peak load 20,000 lbf

3.1.2 Coreflood Cell

The coreflood cell measuring 21 in. (53.3 cm) long with an OD of 3.75 in. (9.53 cm) and wall thickness of 0.75 in. (1.91 cm) is constructed of aluminum (transparent to X-Ray CT scanning). The cell is machined out of a solid cylindrical block of aluminum 7075-T6 to withstand the high temperature and pressure. The maximum operating conditions are 5,000 psig and 200°F. (**Fig. 3.4** and **Fig. 3.5**)

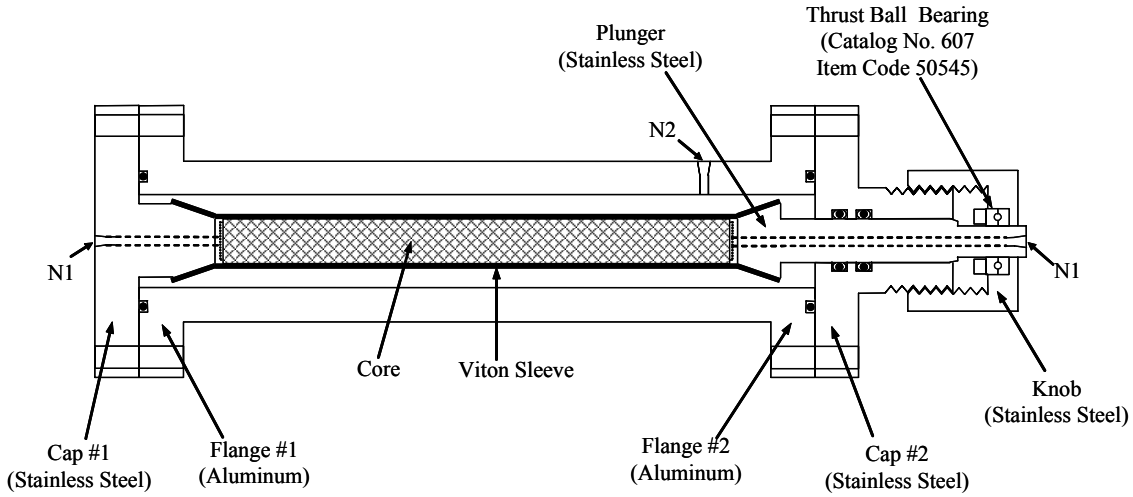

Fig. 3.4—Longitudinal section of coreflood cell (scale approximately 1: 3).

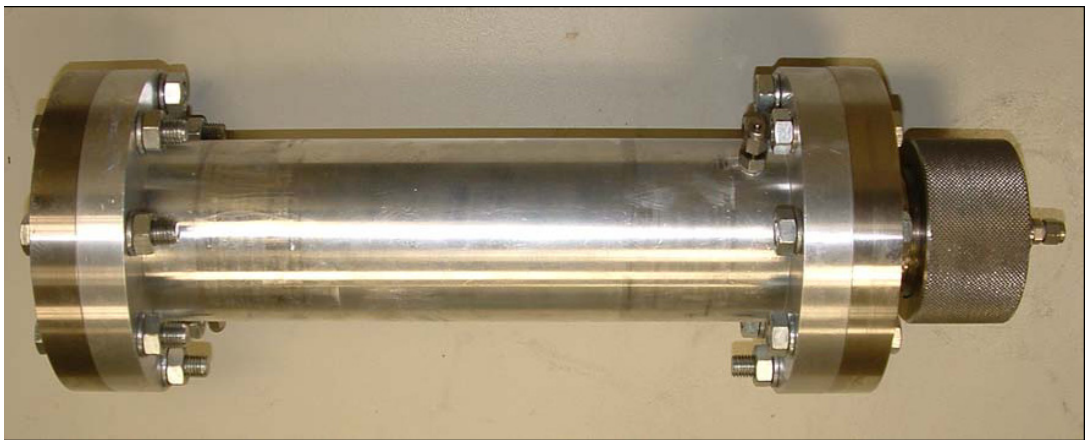

Fig. 3.5—Photograph showing coreflood cell.

An Austin chalk core sample measuring 1 ft (30.5 cm) long and 1 in. (2.54 cm) in diameter is inserted into a Viton Hassler sleeve with both ends secured to plungers in the cell. This is placed inside a *Precision* mechanical convection incubator in a horizontal position for an accurate temperature control as shown in **Fig. 3.6**. In this manner, the desired cell temperature can be obtained. The system is pressurized with nitrogen to test for leaks and then nitrogen is displaced by methane to set the cell with initial conditions for displacement experiments.

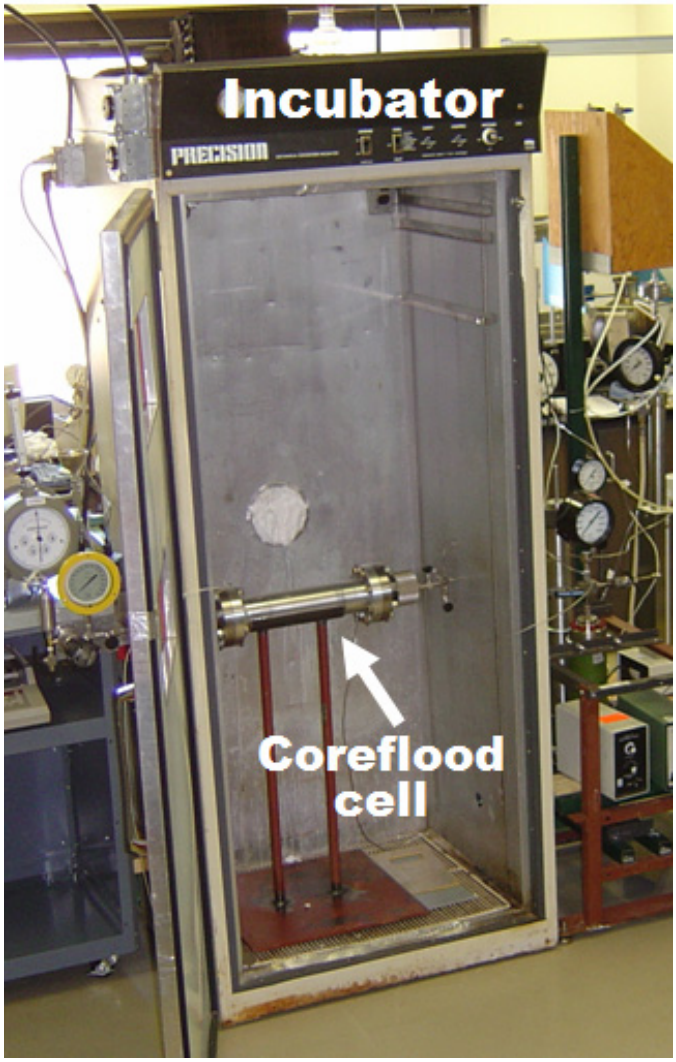

Fig. 3.6—Mechanical convection incubator used to heat the coreflood cell.

3.1.3 The Universal System HD 350 X-Ray CT Scanner

The x-ray CT scanner (**Fig. 3.7**) provides precise determination of core porosity and fluid saturation. The objective of CT scanning is to obtain descriptive images of density variations within the core sample in cross-sectional slices. This non-destructive evaluation process is invaluable to my experiments by imaging porosity and fluid saturations and providing insight into the displacement. CT scanner performs with a speed up to 1 rev/sec and resolution of 6 to 9 line pairs/cm.

Fig. 3.7—Photograph showing Universal System HD 350E X-Ray CT Scanner.

3.1.4. Production and Data Recording System

Produced gas volume and composition are measured using a wet test meter and a *Hewlett Packard* 5890 Series II gas chromatograph with a *Hewlett Packard* 3396A integrator, respectively (**Fig. 3.8**). The cell outlet pressure is set to the desired level with the aid of a *Temco* backpressure regulator. Pressure and temperature readings are recorded in 30-second intervals using a *Hewlett Packard* 34970A data logger in conjunction with a personal computer.

Fig 3.8—Gas chromatograph and data integration system.

3.1.5. Procedure for Displacement Experiments

A typical experiment is conducted as follows:

- Place the Austin chalk core in the thick-walled aluminum coreflood cell described in Fig. 3.4 and Fig. 3.5.
- Place the cell in the mechanical convection incubator at the desire reservoir temperature 65°C to 70°C for an accurate temperature control.
- With the backpressure regulator closed, the coreflood cell is slowly charged up with methane from the accumulator until the desired pressure is reached.
- While injecting methane into the cell, high-temperature *Mobil DTE 26* hydraulic oil is injected into the Hassler sleeve-inner cell wall annulus to maintain an overburden pressure differential of about 300 psi.
- The CO_2 gas mixture is then injected into the cell at a constant rate of 0.25 ml/min.

- Analyze produced gas by using a GC to determine the concentration of the different components in the mixture. Measure cumulative produced gas volume using wet test meter.
- A run is terminated when the methane composition in the produced gas is negligible.

3.2 Compressive Strength Tests

For experiments involving the measurement of compressive strength of the carbonate core, the procedure is the same as described in the foregoing, except that the carbon dioxide stream injection flux is similar to that encountered near the wellbore in the field. **Fig. 3.9** shows a diagram of the apparatus for the dissolution experiments that may potentially lead to changes in the compressive strength of the core.

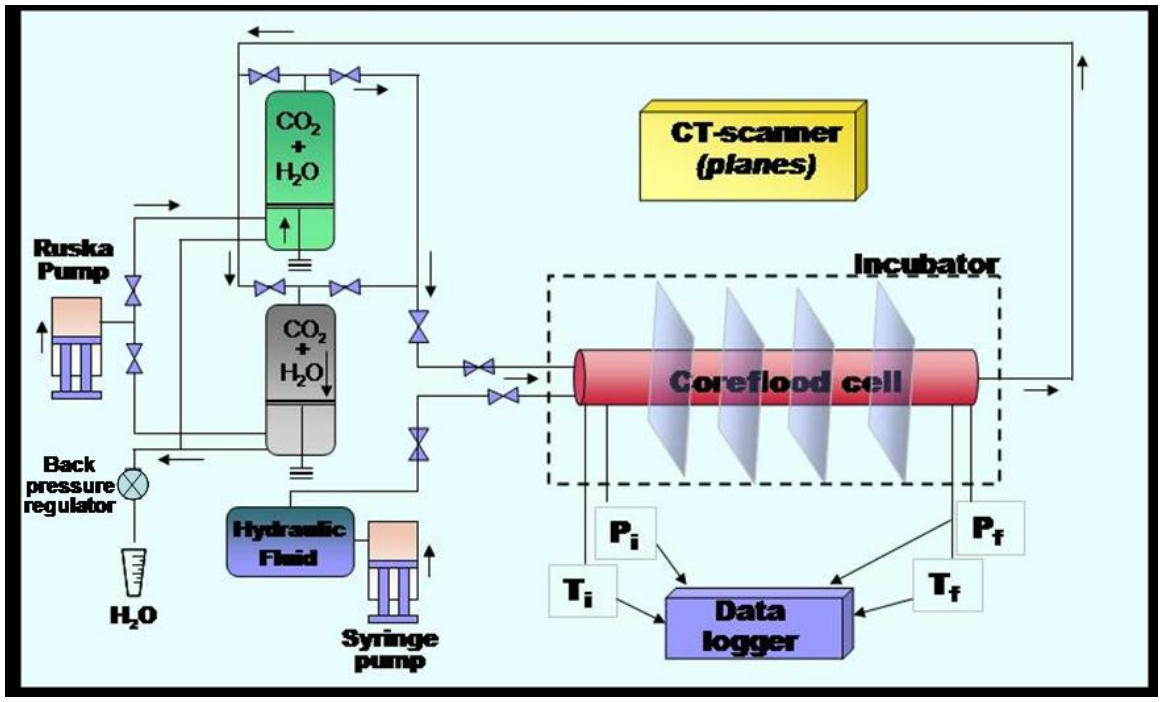

Fig. 3.9—Schematic diagram of experimental apparatus for dissolution experiments.

3.2.1 Dissolution Experiment Design

Runs are performed in such a way that the cell throughput of carbon dioxide simulates near-wellbore throughput. This is achieved through increasing the injection rate and injection time

(weeks). The composition of the fluid injected into the core is CO_2 saturated with water at the same proportion they are emitted from a power plant as previously shown in Table 2.1. It was not possible to include other impurities in the injection gas because the composition of the gas changes over time, and no company could certify the cylinder of gas with the desired composition.

The length of the experiment was determined by scaling the simulation study by Seo and Mamora.[1,13] Their simulation results show that 1.2 MM Tons of CO_2 could be injected into a depleted, 40–acre, 150–ft–thick gas reservoir over 29 years. This amount of CO_2 injected is equivalent to approximately 1,165 moles of CO_2 per square inch of wellbore area. This information was translated into a linear flow through a one-inch diameter, cylindrical core. A total of 914.93 moles would have to be injected through the core to simulate the near-wellbore throughput over the 29 years of injection. This relationship was used to determine the length of the lab experiment to approximately 80 hours, which are equivalent to 30 days of CO_2 injection in the field. A more detailed calculation is presented in Appendix C.

3.2.2. Experimental Procedure

A typical experiment is conducted as follows:

- Fill one of the accumulators with 192cc of distilled water, and add liquid CO_2 from a saturated bottle at 870 psi. Liquid CO_2 is obtained by tilting the bottle as indicated in **Fig. 3.10**. Accumulator is then pressurized at 1,400 psi.
- Place the Austin chalk core in the thick-walled aluminum coreflood cell described in Fig. 3.4 and Fig. 3.5.
- Place the cell in the mechanical convection incubator at the desire reservoir temperature, 65°C for an accurate temperature control.
- With the backpressure regulator closed, the coreflood cell is slowly charged up with methane from a bottle until the desired pressure 1,200 psi is reached.
- While injecting methane into the cell, high-temperature *Mobil DTE 26* hydraulic oil is injected into the Hassler sleeve-inner cell wall annulus to maintain an overburden pressure differential of about 300-500 psi.
- The CO_2 fluid mixture is then injected from the first accumulator into the cell at a high rate varying from 5 to 20 cc/min. The outlet CO_2 stream is collected in the second accumulator and re-injected at the end of the cycle. The back pressure regulator is set at 1,400 psi.
- A run is terminated when 2.587 moles of CO_2 have been injected into the cell, in our case 110 cycles. This is approximately equivalent to 30 days of CO_2 injection in the field.

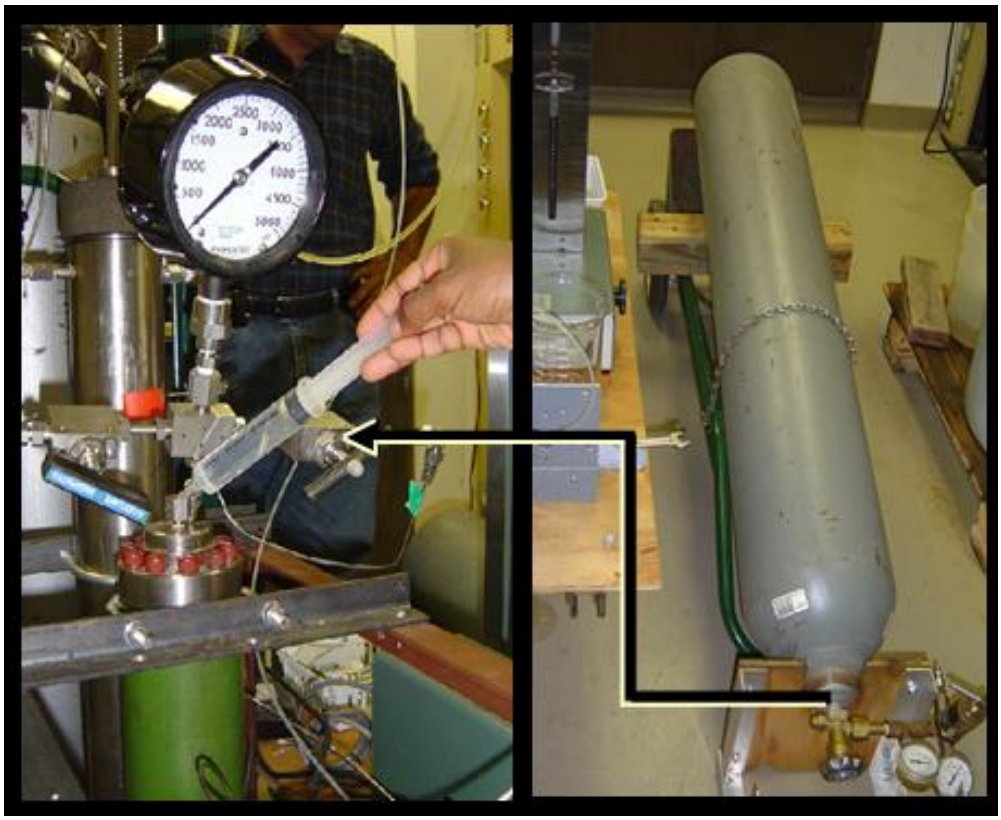

Fig. 3.10 - Preparation of CO_2 mixture for dissolution experiments. Bottle is tilted to obtain liquid CO_2.

After completion of the coreflood run, one–inch diameter and two–inch long rock samples are cut from the core. The unconfined compressive strength (UCS) of the rock samples is then measured by using the *MTS* uniaxial compressive strength apparatus described in Table 3.1 and **Fig 3.11**. The procedure for conducting these tests and for preparing the samples are described in the standard practices ASTM D 4543-01 and ASTM D 2938-95. For each core type, UCS of the original core (not subjected to coreflooding) is measured to obtain the base case. UCS results of flooded cores are then compared against the base case.

In particular, the CT scan analyses are invaluable measuring any changes in core porosity as a result of the more corrosive reactions of the injection stream with the core. Porosity and initial water saturation is measured before the run and compared with values measured at the end of the experiment.

Fig. 3.11—*MTS* uniaxial compressive strength apparatus

CHAPTER IV

EXPERIMENTAL RESULTS

4.1 Displacement Experiment Results

A total of 5 runs at 1,500 psig and 70°C are reported in **Table 4.1.** Three runs injecting Gas A (13.574% CO_2), one of them with initial water saturation of 20% in the core, and two runs injecting Gas B (99.433% CO_2) with zero initial core water saturation. Results indicate that Gas A exhibits higher longitudinal dispersion coefficients and lower C_1 recovery at breakthrough than Gas B.

TABLE 4.1—SUMMARY OF COREFLOOD EXPERIMENTS AT 1,500 PSIG AND 70°C

Injection gas	S_{wi}	OGIP, std L	C_1 recovery at breakthrough, %OGIP	Breakthrough, min	K_L, cm²/min
Gas A	0.0	3.967	80.66%	121.5	0.18
	0.0	4.027	79.46%	102.5	0.19
	0.2	3.227	74.36%	88.5	0.25
Gas B	0.0	3.982	89.90%	112	0.15
	0.0	3.060	88.16%	140	0.13

Prior to every run, core porosity was determined using the CT-scanner. An average porosity of 21% was calculated using the *Voxecalc* software as presented in **Fig. 4.1**. The equations used to measure porosity and saturations are as follows:

$$\phi_{x,y} = \frac{CT_{x,y}^{100\%water} - CT_{x,y}^{dry}}{CT_{water} + 1{,}000} \quad \text{..... (4.1)}$$

where:

$\phi_{x,y}$ is the core porosity at x, y position.

$CT_{x,y}^{100\%water}$ is CT number of core saturated with 100 % water at x, y position.

$CT_{x,y}^{dry}$ is CT number of dry core at x, y position.

CT_{water} is CT number of water used to calculate $CT_{x,y}^{100\%water}$ ($CT_{water} = 0$).

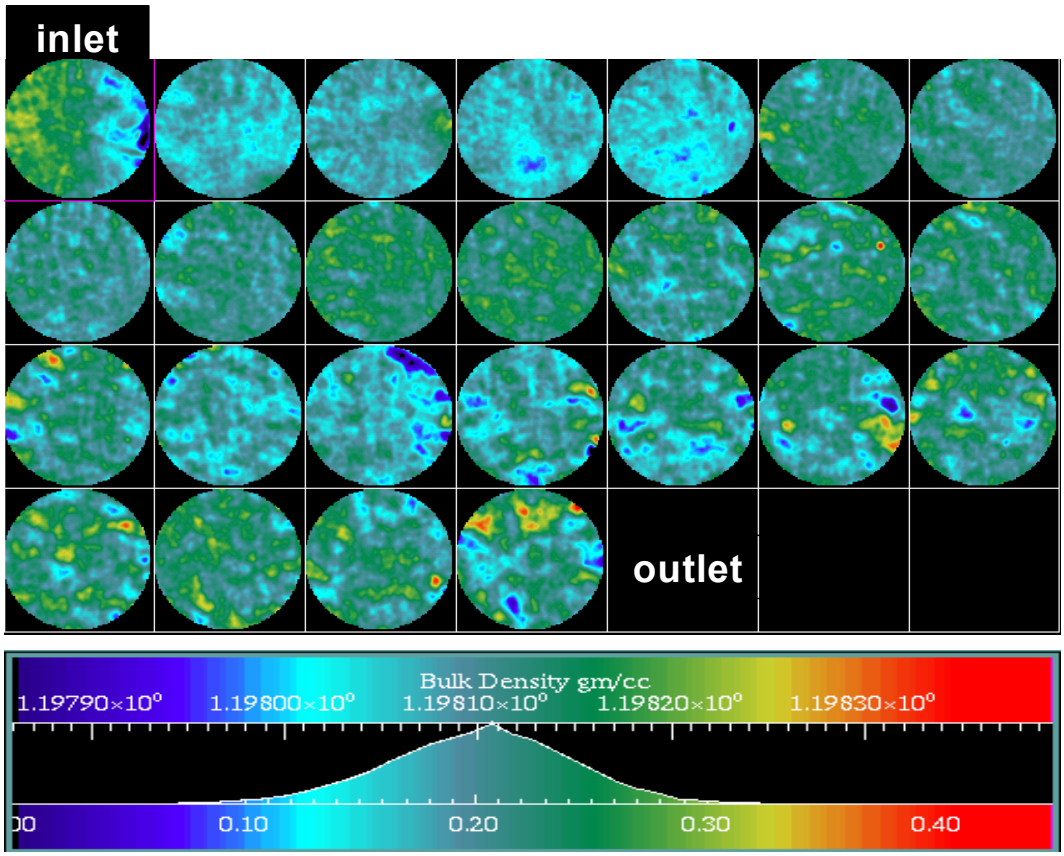

Fig. 4.1—CT scan images of porosity profile using *Voxecalc* software. The core average porosity is 21% as observed in the scale above.

$$S_{x,y}^{water} = \frac{CT_{x,y}^{water} - CT_{x,y}^{dry}}{\phi_{x,y}(CT_{water} + 1{,}000)} \quad \text{..... (4.2)}$$

where:

$S_{x,y}^{water}$ is the core water saturation at x, y position.

$CT_{x,y}^{water}$ is CT number of core partially saturated with water at x, y position.

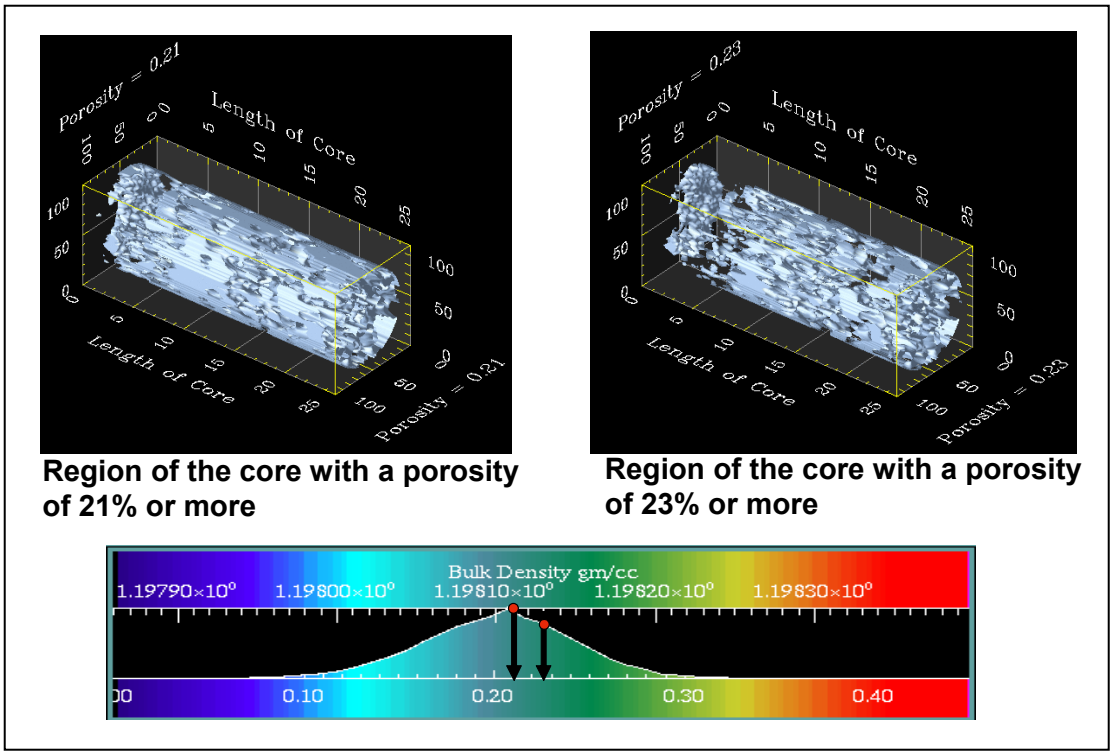

Fig. 4.2—Isosurface images of 3D porosity profiles using *Petro3D*. These images are very helpful to understand the porosity distribution in the core.

A 3D porosity profile was created using *3D-Petro* software to better understand the porosity distribution inside the core (**Fig. 4.2**). Porosity was used to calculate the pore volume, and consequently the *OGIP* with Eq.4.3 and gas recovery at breakthrough for every run.

$$OGIP = \frac{V_p(1 - S_{wi})}{1{,}000\ B_g} \quad \text{..... (4.3)}$$

The coefficients of dispersion of gases A and B were estimated using the convection-dispersion equation previously described in Eq. 2.2. The longitudinal dispersion coefficient was varied to yield the best agreement between experimental data and analytical solution (Eq. 2.4). Calculated profiles of concentration of gases A and B are presented as "best fit" in **Fig. 4.3**. Best-fit lines represent analytical solution for the best value of the coefficient of longitudinal dispersion. Coefficients of dispersion obtained for each run are presented in Table 4.1. These values are, in general, relatively small, ranging from 0.13 to 0.25 cm^2/min.

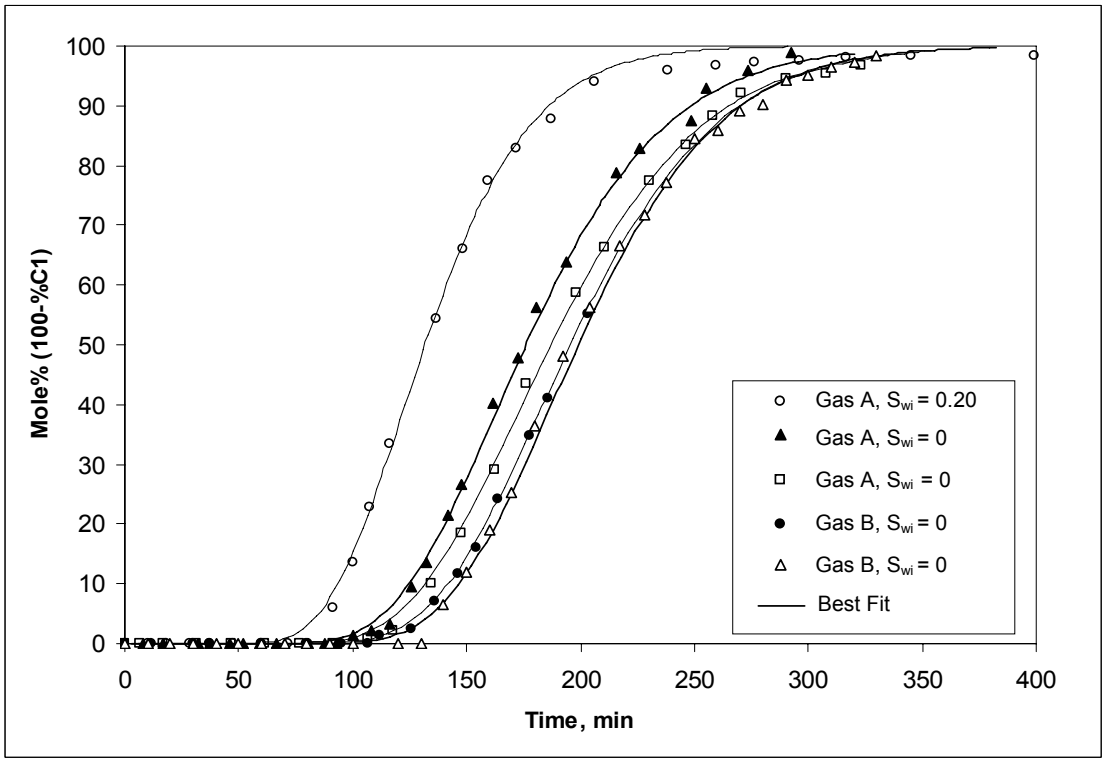

Fig. 4.3—Concentration of the produced gas versus time for runs at 1,500 psig and 70°C.

Comparing our results to those presented in Table 2.2 corresponding to experiments with pure CO_2, the following observations can be pointed out. First, the dispersion coefficient of pure CO_2 at 70°C and 1,500 psig, estimated with linear interpolation from the values presented in Table 2.2 is approximately 0.15 cm^2/min. This value is in good agreement with the dispersion coefficient of Gas B, 0.13 to 0.15 cm^2/min, which contains 99.433 mole % CO_2. Displacement efficiency of Gas B and pure CO_2 are very similar.

Second, the dispersion coefficients for Gas A, 0.18 to 0.25 cm^2/min, is consistently higher than that for pure CO_2 and for Gas B. This result can be better understood by looking at the densities and viscosities of pure CO_2 and Gas A, as well as the phase envelopes at the conditions of the experiment. **Fig. 4.4** and **Fig. 4.5** show densities and viscosities estimated with the software *PVTSim* version 13.0.2. Pure CO_2 exhibits higher density and higher viscosity than Gas A. The phase behavior of pure CO_2 is more liquid-like than Gas A, and thus is more efficient displacing methane in the experiment. In addition, the phase envelope of Gas A (Fig. 3.1) does not exhibit a critical point, indicating that at 70°C and 1,500 psig the fluid is in vapor phase, different from CO_2 that is in supercritical phase.

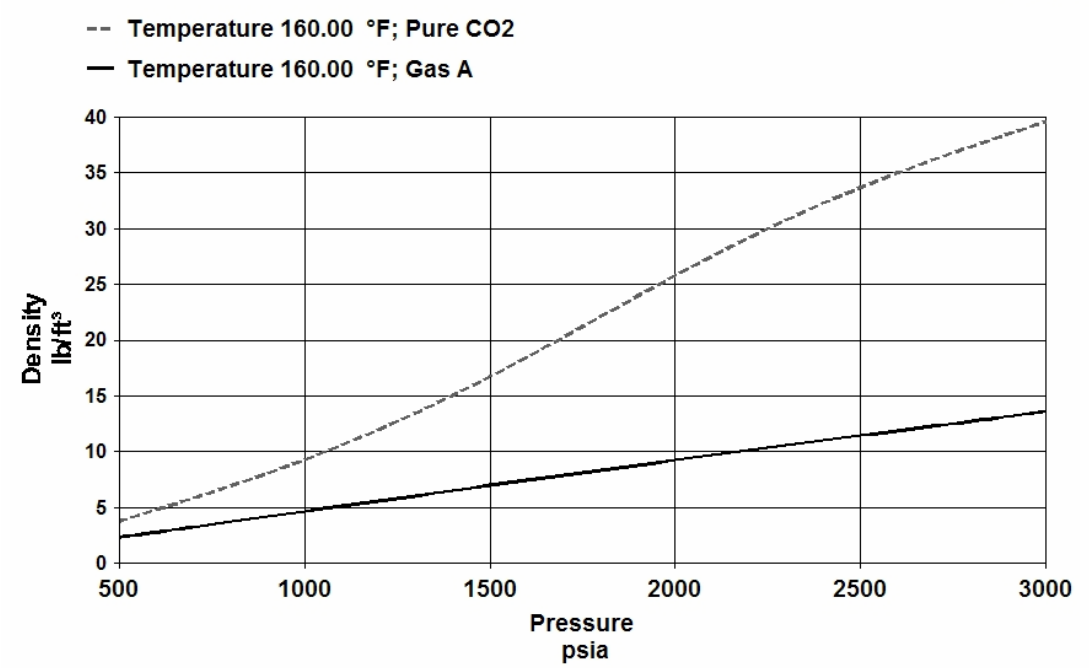

Fig. 4.4—Density diagram with respect to pressure at 160°C (from *PVTSim* 13.0.2).

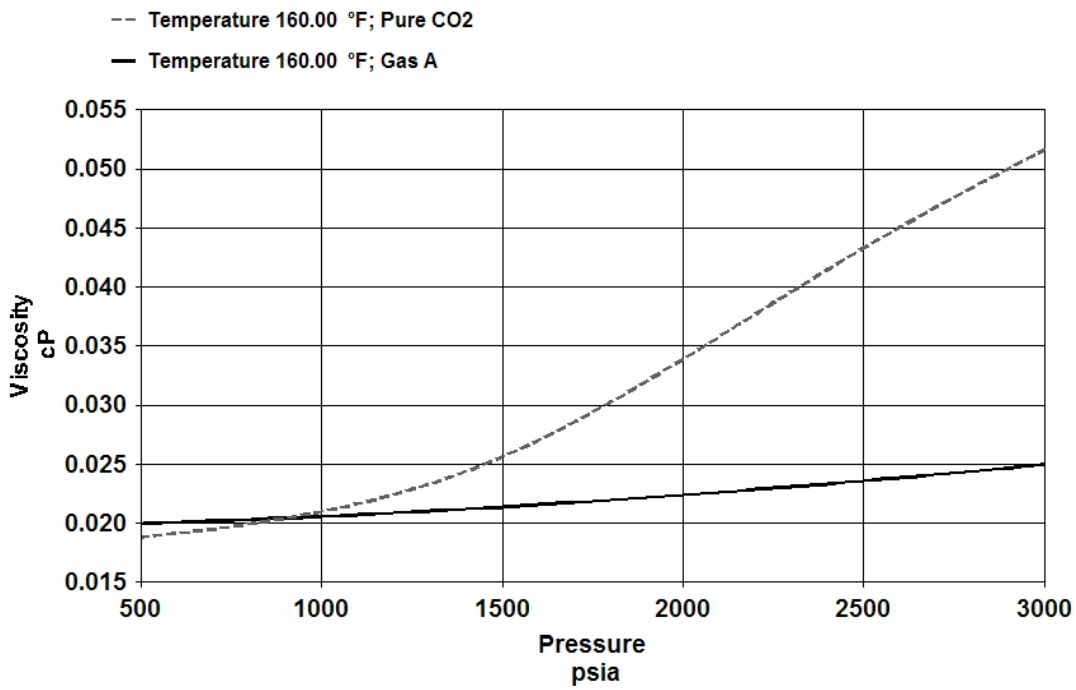

Fig. 4.5—Viscosity diagram with respect to pressure at 160°C (from *PVTSim* 3.0.2). Viscosity of CO_2 is higher than that of Gas A for pressures higher than 1,000 psia.

Breakthrough times vary from 102.5 to 140 min for runs with zero initial water saturation, despite the fact that the water HPLC pump (displacing gases A and B in the accumulator) was set constant to 0.25 ml/min for all runs. This is probably due to cell pressure variations resulting from continuous adjustment of the backpressure regulator during each run. For the run with 20% initial water saturation, the breakthrough time was significantly lower, 88.5 min, due to the reduction in hydrocarbon pore volume compared to zero initial water saturation.

Recovery of methane is lower for Gas A (79-81% OGIP) than for Gas B (88-90% OGIP) and pure CO_2 (ca. 86% OGIP). These results indicate that Gas A exhibits the poorest displacement efficiency, in line with the fact that its longitudinal dispersion coefficient is the largest.

4.2 Compressive Strength Test Results

A total of two marathon dissolution experiments were conducted at 150°F and at an average injection pressure of 1,910 psi. Porosity distribution along the core was measured using the CT-scanner before and after the experiments. After completing approximately 80 hours of CO_2

injection, core samples were dried, extracted from the sleeve, and cut to the desired length as a preparation for the unconfined compressive strength tests.

Porosity was measured using the X-ray CT scanner. First, a pilot image was generated for each core sample (**Fig. 4.6**). This tool was useful to verify the integrity of the sample inside the cell, and to plan the axial plane study. In Fig. 4.6 three sections can be identified for each sample. Average porosity was calculated for each section before and after dissolution experiments.

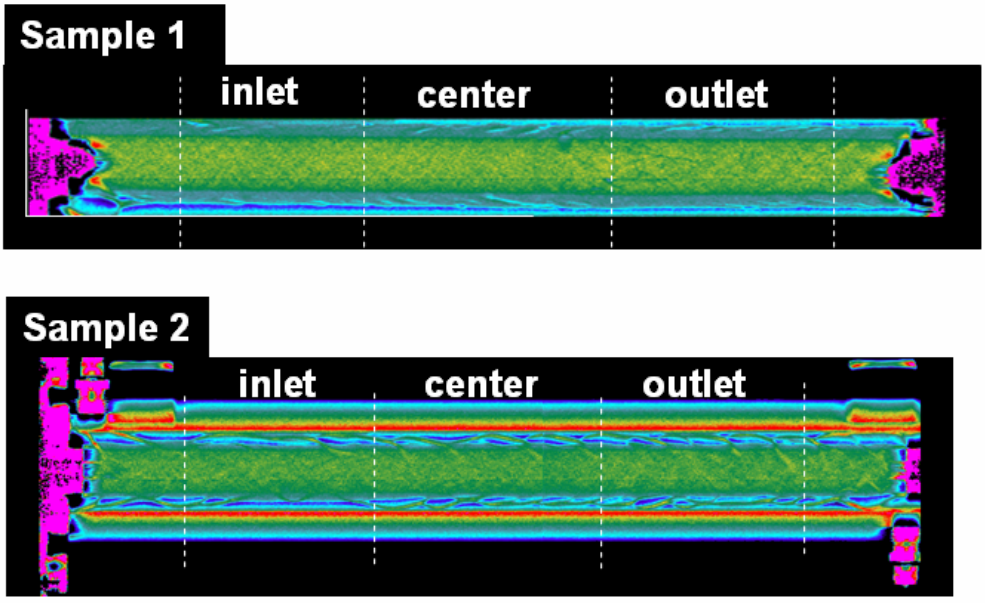

Fig. 4.6—CT scan pilot image for Sample 1 and Sample 2.

CT scan images for Sample 1 are presented in **Fig. 4.7**. The average initial porosity for the central section of the core before the dissolution experiment is 0.200. This section exhibits a small increase in its average porosity up to 0.215 after the dissolution experiments. Evidence of this change is the increase of red spots in images for the final porosity. In the color scale, red represents values for high porosity. Images for the inlet and outlet sections of the core before the dissolution experiments were not available. The outlet section of the core presents a fracture that was possibly caused by the insertion of the core inside the Viton Hassler sleeve with both ends secured to plungers in the cell prior to the experiment.

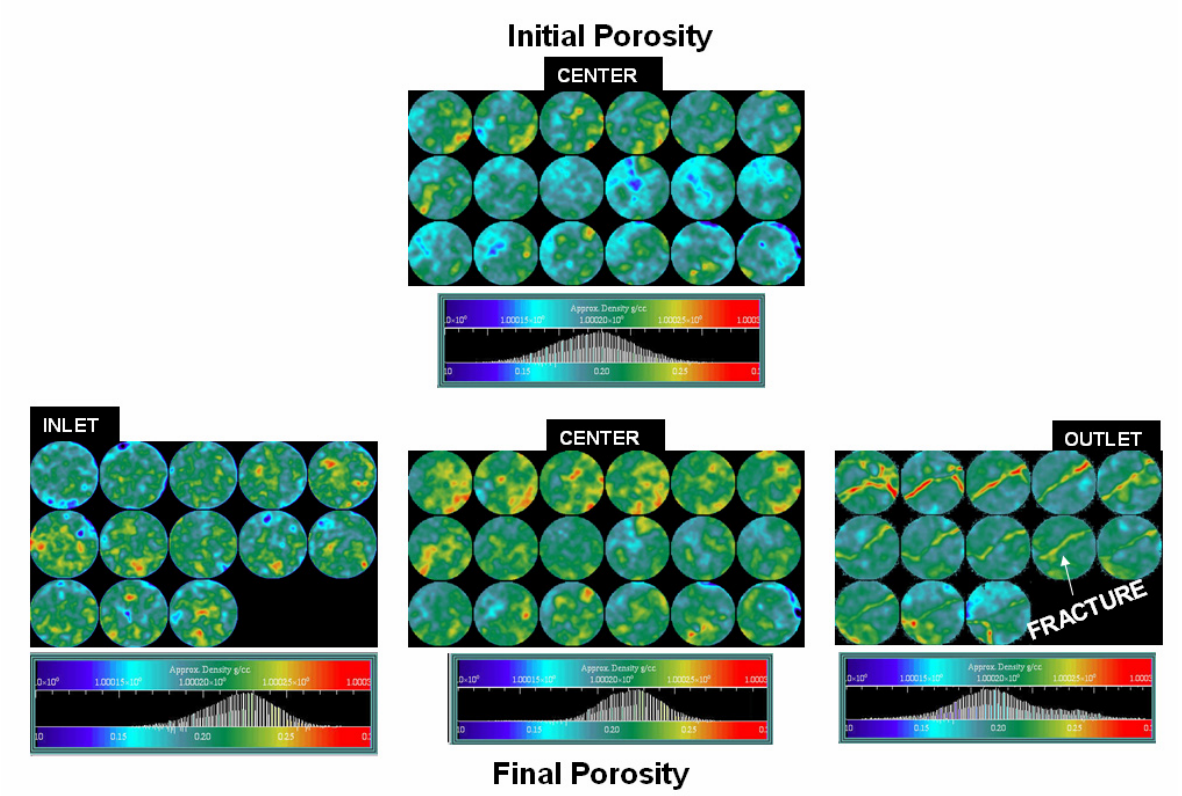

Fig. 4.7—CT scan images of initial and final porosity —Sample 1. Images for the initial porosity were only available for the central section of the core.

CT scan images for Sample 2 are presented in **Fig. 4.8**. The average initial porosity for the inlet, central, and outlet sections of the core before the dissolution experiment are 0.205, 0.225 and 0.230 respectively. After the dissolution experiment, the inlet and central sections exhibit a small increase in its average porosity up to 0.230 and 0.240 respectively; while the outlet section maintains the same average porosity. In general, inlet and center CT scan images for the initial porosity present more blue spots than images for the final porosity. In the color scale, blue represents values for low porosity.

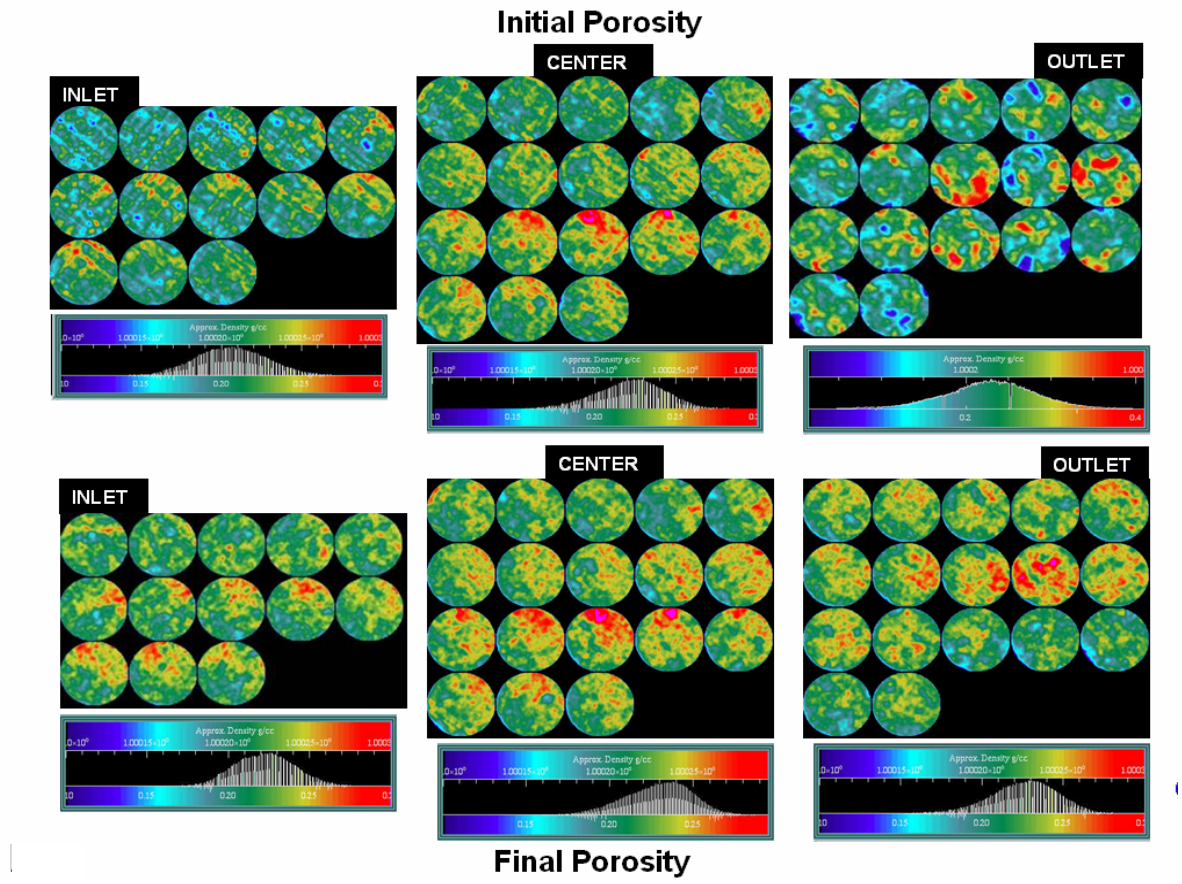

Fig. 4.8—CT scan images of initial and final porosity —Sample 2.

The average porosity for each CT scan image was calculated using *Voxecalc* software and plotted against core length in **Fig. 4.9** and **Fig. 4.10**. The porosity distribution along the core is presented before and after the dissolution experiments. Final porosity values are consistently higher than the initial ones for both core samples. In Fig. 4.10, the increase in porosity is more noticeable in the inlet section of the core. This is probably due to a higher dissolution process in the core inlet. The maximum reduction in rock porosity observed for both core samples was less than or equal to 2.5%.

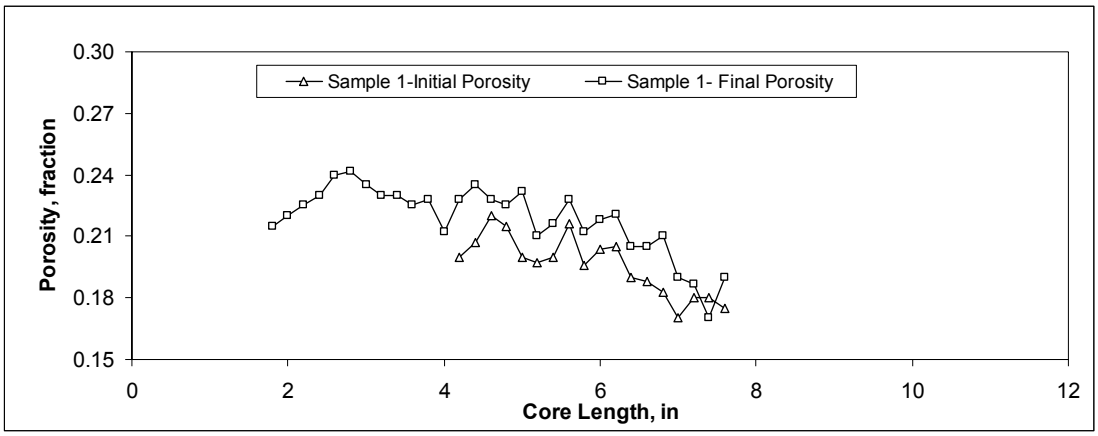

Fig. 4.9—Porosity distribution along the core before and after dissolution experiments for Sample 1.

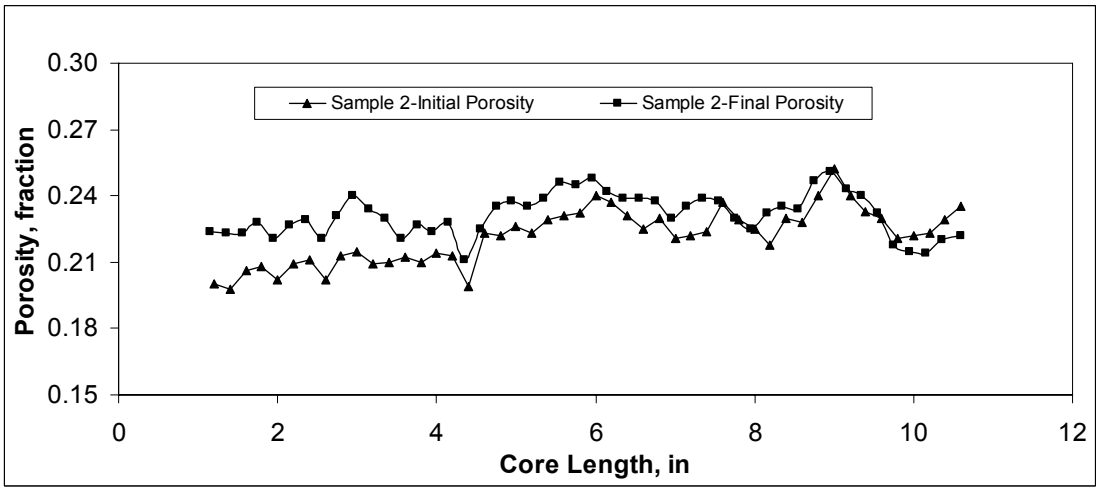

Fig. 4.10—Porosity distribution along the core before and after dissolution experiments for Sample 2.

After completion of each coreflood run, the aluminum cell was open and the core samples were extracted. High pressure, high temperature, and high injection flow rate during coreflood runs caused severe alterations to the sleeve, as presented in **Fig. 4.11**. Both sleeves were carefully cut and core samples were removed from the inside.

Fig. 4.11—Viton Hassler sleeve transformation after coreflood runs.

Fig. 4.12 shows both core samples after dissolution experiments. The outlet section of Sample 1 was fractured as we could anticipate with the CT scan images from Fig. 4.7. Approximately, one third of this core sample was useless for the unconfined compressive strength test. On the contrary, Sample 2 was integer for the following compressive strength test.

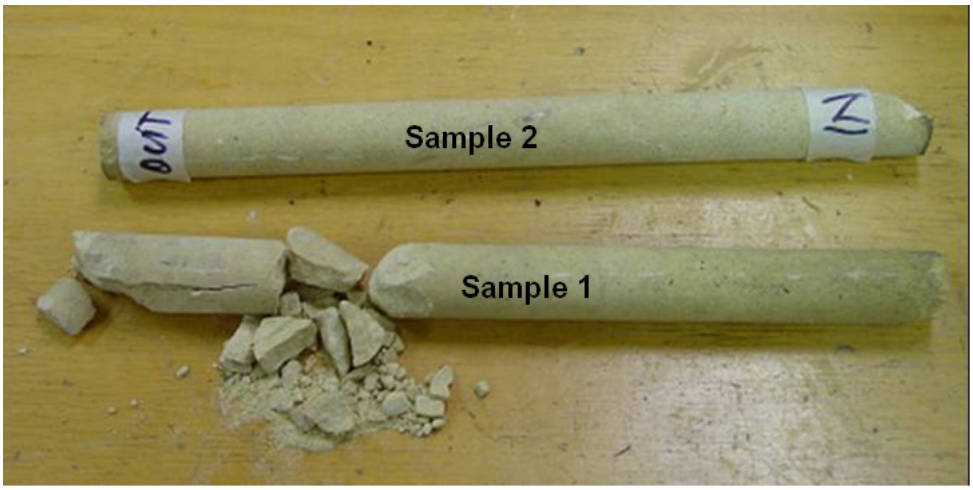

Fig. 4.12—Core samples after coreflood run.

From the three core samples: Base Case, Sample 1 and Sample 2, 11 one–inch diameter and two–inch long rock specimens were cut with a diamond sword and dried for the unconfined compressive strength test. **Fig. 4.13** displays the 11 specimens before the compression test.

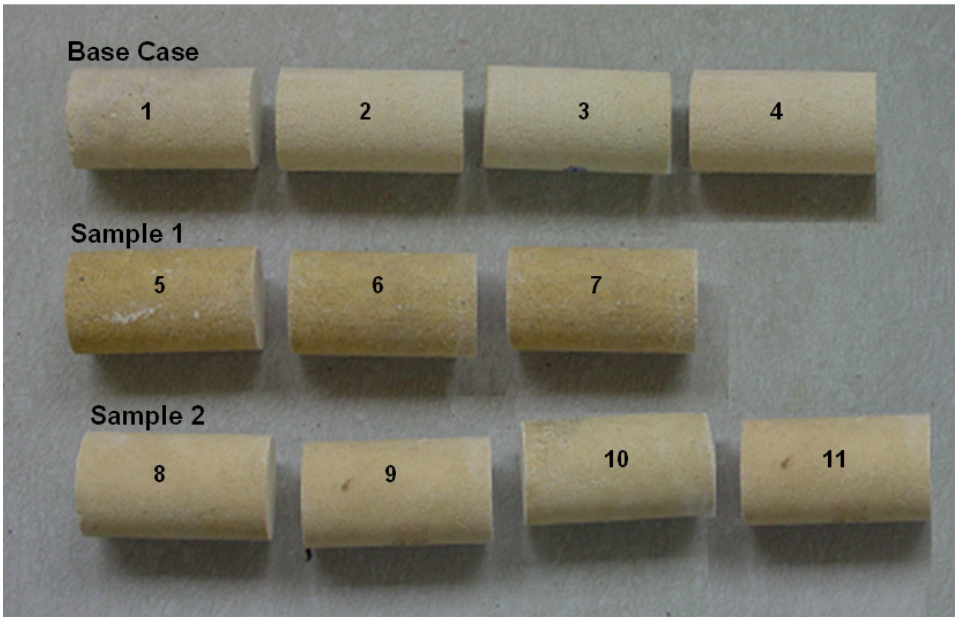

Fig. 4.13—Rock specimens prepared for unconfined compressive strength test.

Unconfined compressive strength test results for the 11 specimens are presented in **Table 4.2**. Tests were performed at room temperature (69 ºF). The moisture condition of all specimens was zero at the time of the test. The rate of loading was constant at 2 lbf/s and the same for all specimens. Results indicate that the integrity of the rock is affected by the long term dissolution experiments. The unconfined compressive strength of the rock was reduced by approximately 30% as a result of the dissolution process from 3,949 ± 966 psi for the base case down to 2729 ± 347 psi for the combined Sample 1 and Sample 2 specimens.

TABLE 4.2— UNCONFINED COMPRESSIVE STRENGTH TEST RESULTS

Description	Specimen	UCS (psi)	Type of failure
Base Case	1	3,459	Columnar
	2	3,547	Columnar
	3	5,395	Cone and Split
	4	3,394	Shear
	mean ± st.dev.	3,949 ± 966	
Sample 1	5	2,951	Columnar
	6	3,110	Cone and Split
	7	2,133	Cone and Split
	mean ± st.dev.	2,731 ± 524	
Sample 2	8	3,077	Columnar
	9	2,688	Cone and Split
	10	2,597	Columnar
	11	2,549	Columnar
	mean ± st.dev.	2,787 ± 255	

The types of failure of the majority of the specimens were columnar or cone-and-split. **Fig. 4.14** presents a good example of a columnar failure. This type of failure indicates that samples were well prepared for the straightness of the elements of the cylindrical surface, the flatness of the end bearing surfaces and the perpendicularity of the end surfaces with the axis of the core.

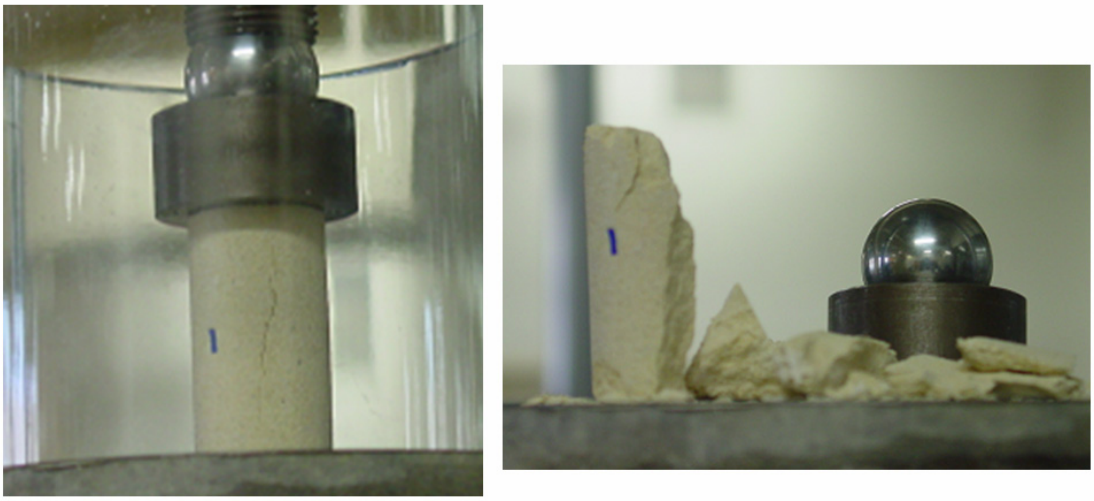

Fig. 4.14─Specimen #1 at the time of failure (columnar failure).

CHAPTER V

SUMMARY, CONCLUSIONS AND RECOMMENDATIONS

5.1 Summary

The main purpose of this research was to evaluate the effect of flue gas impurities on CO_2 displacement efficiency by measuring parameters such as the coefficient of longitudinal dispersion (using the convection/dispersion equation), the natural gas recovery (%OGIP), and the breakthrough time. A secondary objective was to quantify the effect of carbon dioxide injection on calcite dissolution and thus the change in compressive strength**.** Results have been presented and conclusions and recommendations are described next.

5.2 Conclusions

Main conclusions arising from the displacement experiments are summarized as follows.

1. Displacement of methane by Gas A (dehydrated flue gas with CO_2 concentration of 13.574 mole %) at the conditions studied exhibits larger dispersion coefficients, 0.18-0.25 cm^2/min, than displacement by pure CO_2, ca. 0.15 cm^2/min.
2. Impurities appear to have a negligible effect in the displacement of methane by Gas B (CO_2 concentration of 99.433 mole %). Dispersion coefficient of Gas B is 0.13-0.15 cm^2/min.
3. Recovery of methane at breakthrough is higher for Gas B (88-90% OGIP) and pure CO_2 (86% OGIP) than for Gas A (79-81% OGIP). Gas recovery from injection of Gas A is lowest due to the large concentration of N_2 in the gas, resulting in the largest dispersion coefficient of the three injection gases studied.
4. It appears therefore that injection of CO_2 with approximately less than 1 mole % “impurities” would result in practically the same volume of CO_2 being sequestered as injecting pure CO_2. Gas B would have the advantage of being a cheaper separation process compared to pure CO_2 as not all the “impurities” are removed in the case of Gas B.
5. Although separation of CO_2 out of flue gas is a costly process, it appears this is necessary to maximize CO_2 sequestration volume, reduce compression costs of N_2 (approximately 80% of the stream), improve sweep efficiency and gas recovery in the reservoir.

Conclusions from dissolution experiments and unconfined compressive strength tests are summarized as follows:

1. Long term coreflood experiments equivalent to 30 days of CO_2 injection in the field cause a small reduction in the Austin chalk rock porosity less than or equal to 2.5%.
2. The unconfined compressive strength of the Austin chalk rock is significantly reduced by approximately 30% from 3,949 ± 966 psi for the base case down to 2,729 ± 347 psi for the combined Sample 1 and Sample 2 specimens.
3. Although porosity is not significantly reduced by carbon dioxide injection into the Austin chalk formations, unconfined compressive strength results certainly indicate that CO_2 injection will cause weakening of near-wellbore formation rock.

5.3 Recommendations

This study has been performed using Austin chalk core samples. Similar studies using sandstone samples are recommended to determine the impact of rock type on the dispersion of CO_2 in natural gas, and to evaluate rock dissolution and changes in the compressive strength of sandstones.

In these experiments, the Viton Hassler sleeve was severely altered by the long term coreflood experiments. It is recommended to implement a different type of sleeve that can better withstand the conditions of the runs.

NOMENCLATURE

A = cross sectional area, in^2

B_g = formation volume factor of gas (C_1), vol/vol

C = concentration of Gas A or Gas B, mole%

$CT_{x,y}^{dry}$ = CT number of dry core at x, y position

$CT_{x,y}^{100\%water}$ = CT number of core saturated with 100 % water at x, y position

$CT_{x,y}^{water}$ = CT number of core partially saturated with water at x, y position

P_l = peak load, lbf

K_L = coefficient of longitudinal dispersion, cm^2/min

$OGIP$ = original gas (C_1)-in-place, std. Liter

P = pressure, psi

P_e = Peclet number, dimensionless

$\phi_{x,y}$ = core porosity at x, y position

S_{wi} = initial water saturation, fraction

$S_{x,y}^{water}$ = core water saturation at x, y position

t = time, min

t_D = dimensionless time, defined in Eq. 3

T = temperature, ^oC

V_p = pore volume, cm^3

σ_u = unconfined compressive strength, psi

v = insterstitial velocity, cm/min

x = distance from core injection point, cm

x_D = dimensionless distance, defined in Eq. 3

REFERENCES

1. Seo, J.G. and Mamora, D.D.: “Experimental and Simulation Studies of Sequestration of Supercritical Carbon Dioxide in Depleted Gas Reservoirs,” paper SPE 81200 presented at the the 2003 SPE/EPA/DOE Exploration and Production Environmental Conference, San Antonio, Texas, 10–12 March.
2. Khilyuk, L.F., Chilingar, G.V., and Al-Hamdan, M.R.: “Global Warming and Petroleum Production” paper SPE 83506 presented at the 2003 SPE Western Regional/AAPG Pacific Section Joint Meeting, Long Beach, California, 19–24 May.
3. Halloway, S. and van der Straaten, R.: “The Joule II Project – The Underground Disposal of Carbon Dioxide,” *Energy Conversion Management* (1996) **37**, No. 6–8, 1149.
4. United Nations Framework Convention on Climate Change (UNFCC), Report of the Conference of the Parties, Kyoto, Japan, 10-11 December 1997.
5. Le Gallo, Y., Couillens, P., and Manai, T.: “CO_2 Sequestration in Depleted Oil or Gas Reservoirs,” paper SPE 74104 presented at the 2002 SPE International Conference on Health, Safety and Environment in Oil and Gas Exploration and Production, Kuala Lumpur, Malaysia, 20–22 March.
6. Orr, F.: “Storage of Carbon Dioxide in Geologic Formations,” JPT (September 2004) **56**, No. 9, 90-97.
7. Korbul, R. and Kaddour, A.: “Sleipner Vest CO_2 Disposal – Injection of Removed CO_2 into the Utsira Formation,” *Energy Conversion and Management* (1995) **36**, No. 6–9, 509.
8. Malik, Q.M. and Islam, M.R.: “CO_2 Injection in the Weyburn Field of Canada: Optimization of Enhanced Oil Recovery and Greenhouse Gas Storage with Horizontal Wells,” paper SPE 59327 presented at the 2000 SPE/DOE Improved Oil Recovery Symposium, Tulsa, 3–5 April.
9. Mamora, D.D. and Seo, J.G.: “Enhanced Gas Recovery by Carbon Dioxide Sequestration in Depleted Reservoirs,” paper SPE 77347 presented at the 2002 SPE Annual Technical Conference and Exhibition, San Antonio, Texas, 29 September–2 October.
10. Zhang, P.Y., Kharghoria, A., Zhong, He, and Datta-Gupta, A.: “Effect of CO_2 Impurities on Gas-Injection EOR Processes,” SPE paper 89477 presented at the 2004 SPE/DOE Fourteenth Symposium on Improved Oil Recovery, Tulsa, Oklahoma, 17–21 April.
11. *The Prospects for CO_2 Capture and Storage*, International Energy Agency, Paris (December 2004).

12. Nguyen, D.N.: “Carbon Dioxide Geological Sequestration: Technical and Economic Review,” paper SPE 81199 presented at the 2003 SPE/EPA/DOE Exploration and Production Environmental Conference, San Antonio, Texas, 10–12 March.
13. Seo, J.G.: “Experimental and Simulation Studies of Sequestration of Supercritical Carbon Dioxide in Depleted Gas Reservoirs,” PhD dissertation, Texas A&M U., College Station, Texas (2004).
14. Nogueira, M.C. and Mamora, D.D.: “Effect of Flue Gas Impurities on the Process of Injection and Storage of CO_2 in Depleted Gas Reservoirs,” paper SPE 94906 presented at the 2005 SPE/EPA/DOE Exploration and Production Environmental Conference, Galveston, Texas, 7–9 March.
15. “Geochemical Aspects of CO_2 Sequestration,” *Chemical Geology*, (2005) **217**, No. 3–4, 183–186.
16. Morse, J.W.: “The Kinetics of Calcium Carbonate Dissolution and Precipitation in Carbonates,” Mineralogy and Chemistry, R.J. Reeder, ed., Mineralogical Society of America, Washington, D.C. (1983) 227–264.
17. Morse, J.W. and Arvidson R.S.: “Dissolution Kinetics of Major Sedimentary Carbonate Minerals,” *Earth Science Rev*, (2002) **58**, 51-84.
18. Morse, J.W. and Mackenzie F.T.: *Geochemistry of Sedimentary Carbonates*, Elsevier, Amsterdam, 707.
19. Grigg, R.B.: “State of the Industry in CO_2 Flood,” paper SPE 38849 presented at the 1997 SPE Annual Technical Conference, San Antonio, Texas, 5–8 October.
20. Izgec, O. and Demiral, B.: “CO_2 Injection in Carbonates,” paper SPE 93773 presented at the 2005 SPE Western Regional Meeting, Irvine, California, 30 March–1 April.
21. Egermann P., Bazin, B., and Vizika, O.: “An Experimental Investigation of the Reaction-Transport Phenomena During CO_2 Injection,” paper SPE 93674 presented at the 2005 SPE Middle East Oil & Gas Show and Conference, Bahrain, 12–15 March.
22. Tristan P., Grigg, R.B., McPherson, B.J., Svec, R.K., and Lichtner, P.C.: “Evaluation of CO2-Brine-Reservoir Rock Interaction with Laboratory Flow Tests and Reactive Transport Modeling,” paper SPE 80228 presented at the 2003 SPE International Symposium on Oilfield Chemistry, Houston, 5–7 February.
23. Knauss, K.G. Johnson J.W. and Steefel, C.I.: “Evaluation of the Impact of CO_2, Co-contaminant Gas, Aqueous Fluid and Reservoir Rock Interactions on the Geologic Sequestration of CO_2,” *Chemical Geology*, (2005) **217**, No. 3–4, 339–350.

24. Goodman, R.E.: *Introduction to Rock Mechanics*, second edition, J.Wyley & Sons, Inc. New York City (1989) 55-62.
25. “Geotechnical Design Summary Report,” Parsons Brinckerhoff/Morrison Knudsen Joint Venture, (April 1992). (Personal Collection M. Nogueira de Mago)

APPENDIX A

EXPERIMENTAL DATA FOR DISPLACEMENT EXPERIMENTS

Duration for displacement experiments was approximately 5 hours. Breakthrough time occurred generally during the first two hours. The following tables show the composition (mol %) of the produced gas over time and the cumulative gas produced. **Table A.1** shows results for the second run with a breakthrough of 88.5 min, a C_1 produced at breakthrough 2.40 L.

TABLE A.1—EXPERIMENTAL DATA FOR RUN #2, GAS A INJECTED AT 1,500 PSI AND 70°C AND 20% INITIAL WATER SATURATION

t (min)	Total flow (L)	CO_2%	O_2%	N_2%	C_1%	(100%-C_1%)
0	0	0	0	0	100	0
10.50	0.15	0	0	0	100	0
18.50	0.41	0	0	0	100	0
28.50	0.72	0	0	0	100	0
37.50	1.00	0	0	0	100	0
47.50	1.32	0	0	0	100	0
59.78	1.71	0	0	0	100	0
71.50	2.08	0	0	0	100	0
80.50	2.23	0	0	0	100	0
88.50	2.40	0	0	5.96	94.04	5.96
100.50	3.01	0	0.69	12.93	86.34	13.66
107.50	3.29	0	1.37	21.57	77.06	22.94
116.50	3.56	0	2.1	32.04	66.46	33.54
136.50	4.03	1.28	3.34	49.22	45.73	54.27
148.50	4.45	2.09	4.07	59.77	34.02	65.98
159.50	4.72	3.63	4.69	68.97	22.65	77.35
171.50	5.03	4.63	5.02	73.28	17.24	82.77
187.50	5.43	5.26	5.27	77.3	12.12	87.88
206.50	6.10	7.15	5.61	80.91	6.11	93.89
238.50	6.81	7.79	5.74	82.37	4.10	95.90
259.50	7.38	8.54	5.75	82.42	3.26	96.74
276.50	7.78	8.8	5.77	82.6	2.79	97.21
296.50	8.25	8.87	5.78	82.68	2.32	97.68
316.50	8.68	9.14	5.81	83.05	2.00	98.00
345.00	10.32	9.13	5.83	83.27	1.74	98.26
399.50	10.57	9.48	5.82	83.19	1.57	98.43

Table A.2 shows results for the third run with a breakthrough of 100.5 min, and a C_1 produced at breakthrough 3.20 L.

TABLE A.2—EXPERIMENTAL DATA FOR RUN #3, GAS A INJECTED AT 1,500 PSI AND 70°C AND 0% INITIAL WATER SATURATION

t (min)	Total flow (L)	CO_2%	O_2%	N_2%	C_1%	(100%-C_1%)
0.00	0					
8.00	0.02	0	0	0	100	0
17.00	0.68	0	0	0	100	0
32.00	0.85	0	0	0	100	0
37.50	1.48	0	0	0	100	0
46.00	1.51	0	0	0	100	0
51.95	1.75	0	0	0	100	0
59.00	2.03	0	0	0	100	0
66.50	2.29	0	0	0	100	0
80.42	2.67	0	0	0	100	0
87.42	3.08	0	0	0	100	0
93.00	3.12	0	0	0	100	0
100.50	3.20	0.50	0	0.78	98.72	1.28
108.22	3.27	0.58	0	1.39	97.88	2.12
116.25	3.43	1.14	0.15	2.10	96.61	3.39
125.75	3.73	3.73	0.34	5.30	90.43	9.57
132.00	4.01	0.77	0.77	12.08	86.37	13.63
141.67	4.26	1.18	1.22	18.95	78.51	21.49
147.50	4.46	1.83	1.51	23.24	73.43	26.57
161.50	4.77	2.31	2.33	35.58	59.78	40.22
172.75	5.02	2.81	2.76	42.03	52.26	47.74
180.50	5.29	3.49	3.27	49.33	43.78	56.22
193.50	5.62	4.06	3.73	55.90	36.20	63.80
215.50	6.43	6.09	4.59	68.18	21.12	78.88
226.00	6.72	6.51	4.84	71.58	17.03	82.97
248.50	7.22	6.90	5.13	75.55	12.39	87.61
255.50	7.70	8.95	5.33	78.70	7.02	92.98
273.50	8.03	10.64	5.60	79.80	3.96	96.04
292.50	8.70	11.06	5.74	82.18	1.01	98.99

Table A.3 shows results for the fourth run with a breakthrough of 117.5 min, and a C_1 produced at breakthrough 3.20 L.

TABLE A.3—EXPERIMENTAL DATA FOR RUN #4, GAS A INJECTED AT 1,500 PSI AND 70°C AND 0% INITIAL WATER SATURATION

t (min)	Total flow (L)	CO_2%	O_2%	N_2%	C_1%	(100%-C_1%)
0.00	0.00	0	0	0	100	0
6.50	0.11	0	0	0	100	0
16.50	0.54	0	0	0	100	0
31.50	0.97	0	0	0	100	0
46.50	1.35	0	0	0	100	0
61.50	1.71	0	0	0	100	0
76.50	2.08	0	0	0	100	0
91.50	2.56	0	0	0	100	0
106.50	2.93	0	0	0.73	99.27	0.73
117.50	3.20	0.06	0	1.99	97.95	2.05
134.50	3.76	5.37	0.08	4.70	89.85	10.15
147.50	4.34	0.83	1.04	16.69	81.44	18.56
162.50	4.43	2.31	1.59	25.11	70.94	29.06
176.50	4.68	3.66	2.41	37.21	56.59	43.41
198.50	5.25	4.46	3.25	50.96	41.21	58.79
210.50	5.58	5.01	3.80	57.34	33.83	66.17
230.50	5.89	6.04	4.49	66.86	22.61	77.39
246.50	6.41	7.10	4.85	71.57	16.47	83.53
258.50	6.75	7.77	5.14	75.44	11.59	88.41
270.50	7.34	10.02	5.28	77.12	7.78	92.22
290.50	7.74	8.97	5.50	79.89	5.50	94.50
307.50	8.25	9.31	5.53	80.61	4.52	95.49
323.50	8.89	10.61	5.60	80.90	3.39	96.61

Table A.4 shows results for the fifth run with a breakthrough of 112 min, and a C_1 produced at breakthrough 3.58 L.

TABLE A.4—EXPERIMENTAL DATA FOR RUN #5, GAS B INJECTED AT 1,500 PSI AND 70°C AND 0% INITIAL WATER SATURATION

t (min)	Total flow (L)	CO_2%	O_2%	N_2%	C_1%	(100%-C_1%)
0.00	0.00	0.00	100.00	0.00	0.00	0.00
12.00	0.11	0.00	100.00	12.00	0.11	0.00
30.00	1.00	0.00	100.00	30.00	1.00	0.00
37.00	1.47	0.00	100.00	37.00	1.47	0.00
60.00	1.90	0.00	100.00	60.00	1.90	0.00
80.00	2.45	0.00	100.00	80.00	2.45	0.00
95.00	2.93	0.00	100.00	95.00	2.93	0.00
107.00	3.32	0.00	100.00	107.00	3.32	0.00
112.00	3.58	1.314	98.69	112.00	3.58	1.314
126.00	3.90	2.53	97.47	126.00	3.90	2.53
136.00	4.14	7.07	92.93	136.00	4.14	7.07
146.00	4.33	11.67	88.33	146.00	4.33	11.67
154.00	4.62	15.98	84.02	154.00	4.62	15.98
164.00	4.85	24.18	75.82	164.00	4.85	24.18
178.00	5.24	34.84	65.16	178.00	5.24	34.84
186.00	5.42	41.16	58.84	186.00	5.42	41.16
203.00	6.17	55.03	44.97	203.00	6.17	55.03

Table A.5 shows results for the sixth run with a breakthrough of 140 min, and a C_1 produced at breakthrough 3.15 L.

TABLE A.5—EXPERIMENTAL DATA FOR RUN #6, GAS B INJECTED AT 1,500 PSI AND 70°C AND 0% INITIAL WATER SATURATION

t (min)	Total flow (L)	CO_2%	C_i%
0.00	0.00	0	100.00
10.00	0.24	0	100.00
20.00	0.41	0	100.00
30.00	0.57	0	100.00
40.00	0.65	0	100.00
50.00	0.71	0	100.00
60.00	0.77	0	100.00
70.00	0.95	0	100.00
80.00	1.29	0	100.00
90.00	1.34	0	100.00
100.00	1.51	0	100.00
120.00	1.92	0	100.00
130.00	2.42	0	100.00
140.00	3.15	6.50	93.50
150.00	3.46	11.97	88.03
160.00	3.84	19.00	81.00
170.00	4.24	25.16	74.84
180.00	4.8	36.34	63.66
192.00	5.42	48.21	51.79
204.00	6.04	56.20	43.80
217.00	6.57	66.61	33.39
228.00	7.46	71.63	28.37
238.00	7.95	77.28	22.72
250.00	8.34	84.51	15.49
260.00	8.87	85.85	14.15
270.00	9.11	89.18	10.82
280.00	9.58	90.27	9.73
290.00	9.92	94.17	5.83
300.00	10.12	95.20	4.80
310.00	10.71	96.58	3.42
320.00	11.00	97.28	2.72
330.00	11.21	98.41	1.59

APPENDIX B

VBA CODES FOR DISPLACEMENT EXPERIMENTS

The following VBA function was written to calculate the analytical concentration of the produced gas described in **Eq. 2.3** by solving the convection-dispersion equation. All other calculations were made with a spreadsheet.

```
Function erff(x As Double) As Double
If x < 0 Then
erff = Sgn(x) * erf(Abs(x))
Else
erff = erf(x)
End If
End Function
```

APPENDIX C

DISSOLUTION EXPERIMENT DESIGN—CALCULATIONS

In dissolution experiments the cell throughput of carbon dioxide simulates near-wellbore throughput. The length of the experiment was determined by scaling the simulation study by Seo and Mamora.[1,13] **Table C1** shows the data and results for this CO_2 sequestration simulation.

TABLE C.1—RESERVOIR DATA AND RESULTS FOR SIMULATION STUDY BY SEO AND MAMORA[1,13]

Reservoir Data	
Area, acres	40
Simulation pattern	0ne eighth five spot
Thickness, ft	150
Porosity, fraction	0.23
X,Y Permeability, md	50
Z permeability, md	5
Initial water saturation, fraction	0
Temperature, °F	152
Original pressure, psi	3,045
Depth, ft	7,000
Simulation Results	
CO_2 sequestered, MM Tons	1.2
Injection rate, STB/D	200
Injection time, yr	29

Calculations

Using the simulation data provided in **Table C.1**, calculate the area along the wellbore that will be in contact with the injected gas. Assume a wellbore radius of 0.345 ft.

$$Area_{simulation} = 2\pi rL = 2(3.1416)(0.345\,ft)(150\,ft) = 325.16\,ft^2$$

Calculate the amount of CO_2 moles injected through all the sequestration process in the simulation.

$$Moles_{simulation} = \frac{mass_1}{MW_{CO_2}} = 1.2MM\ Tons\ CO_2\left(\frac{2{,}000lbm}{1Ton}\right)\left(\frac{lbmol}{44lbm}\right) = 54.545MM\ moles\ CO_2$$

For the lab calculations, determine the cross sectional area of the core that will be in contact with the injected gas.

$$Area_{lab} = \pi r^2 = (3.1416)(0.5in)^2\left(\frac{1ft}{12in}\right)^2 = 0.00545\,ft^2$$

Calculate the amount of CO_2 moles that need to be injected through the cross sectional area of the core to scale 29 years of the simulation study.

$$Moles_{lab} = Moles_{simulation}\left(\frac{Area_{lab}}{Area_{simulation}}\right) = 54.545*10^6\left(\frac{0.00545}{325.16}\right) = 914.93 moles\ CO_2$$

The maximum amount of CO_2 that the accumulator can hold is 0.0235 moles at room temperature and 870 psi. It will take approximately three years to inject this amount of moles. The relationship between the moles of CO_2 and the years of injection was used to determine the length of the lab experiment to approximately 80 hours, which are equivalent to 30 days of CO_2 injection in the field.

VITA

Name: Marjorie C. Nogueira de Mago

Place of Birth: Caracas, Venezuela

Contact Information: 3116 TAMU - 507 Richardson Building
College Station TX, 77843-3116

Education: B.S., Chemical Engineering (November 2002)
Simon Bolivar University, Caracas, Venezuela

M.S., Petroleum Engineering (August 2005)
Texas A&M University, College Station, Texas

Professional Affiliations: Society of Petroleum Engineers, Member

Papers: Nogueira, M.C. and Mamora, D.D.: "Effect of Flue Gas Impurities on the Process of Injection and Storage of CO_2 in Depleted Gas Reservoirs," paper SPE 94906 presented at the 2005 SPE/EPA/DOE Exploration and Production Environmental Conference, Galveston, Texas, 7–9 March.